TURBO AND TITO

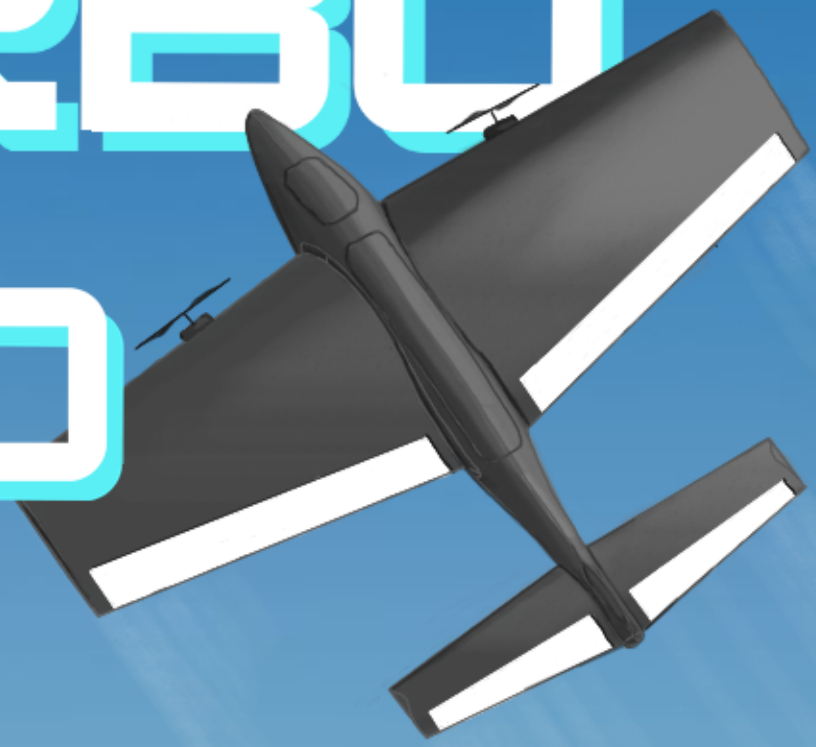

Queen's University

Queen's AEROSPACE. DESIGN TEAM

AIAA Design Report 2026

Table of Contents

1 Executive Summary **3**

2 Management Summary **4**
2.1 Team Organization . . . 4
2.2 Schedule . . . 4
2.3 Budget . . . 5

3 Conceptual Design **6**
3.1 Problem Statement and High Level Overview . . . 6
3.2 Staging and Mission Specifications . . . 6
3.3 Mission 1 Description and Scoring . . . 7
3.4 Mission 1 Design Requirements Analysis . . . 7
3.5 Mission 2 Description and Scoring . . . 8
3.6 Mission 2 Design Requirements Analysis . . . 8
3.7 Mission 3 Description and Scoring . . . 9
3.8 Mission 3 Design Requirements Analysis . . . 9
3.9 Ground Mission Description and Scoring . . . 10
3.10 Ground Mission Design Requirements Analysis . . . 10
3.11 Non-mission Based Requirements . . . 10
3.12 Scoring Sensitivity Analysis . . . 12
3.13 Configuration Selection . . . 13

4 Preliminary Design **15**
4.1 Design Process and Analysis . . . 15
4.2 Aircraft Performance . . . 21
4.3 Aircraft Stability . . . 27
4.4 Mission Payloads . . . 29

5 Detail Design **31**
5.1 Dimensional Parameters . . . 31
5.2 Structural Characteristics . . . 32
5.3 Systems Selection and Integration . . . 37
5.4 CFD Design Verification . . . 38
5.5 Weight and Balance . . . 38
5.6 Aircraft Performance . . . 39
5.7 Mission Performance . . . 40
5.8 Drawing Package . . . 41

6 Manufacturing Plan **44**
6.1 Manufacturing Methods . . . 44
6.2 Material and Manufacturing Method Selection . . . 45
6.3 Manufacturing Execution . . . 46

7 Testing Plan **48**
7.1 Ground Testing . . . 49
7.2 Flight Testing . . . 52

8 Performance Results **54**
8.1 Subsystem Performance . . . 54

9 Bibliography **58**

Nomenclature			
Symbols		***Subscripts***	
AR	Aspect ratio	a	aileron
b	Span	e	elevator
c	Chord	r	rudder
C_d	Drag coefficient	***Competition Scoring Values***	
C_{d0}	Zero-lift drag coefficient	B_L	Banner length
C_l	Lift coefficient	CC_c	Total cargo the plane can carry
D	Drag	CC_p	Total passengers the plane can carry
e	Oswald's efficiency	C_c	Cargo operating cost per lap (2)
m	Mass	C_e	Base operating cost per lap (10)
μ	Ground rolling friction coefficient	C_p	Passenger operating cost per lap (0.5)
n	Load factor	E_F	Efficiency factor (battery capacity in Wh divided by 100)
ρ	Air density	L_1	Expected completable laps in Mission 1
Re	Reynolds number	L_2	Expected completable laps in Mission 2
S	Planform area	L_3	Expected completable laps in Mission 3
T	Thrust	l_{c1}	Fixed income per cargo (10)
V	Velocity	l_{c2}	Income per cargo per lap (8)
W	Weight	l_{p1}	Fixed income per passenger (6)
WS	Wing span	l_{p2}	Income per passenger per lap (2)
X_{NP}	Neutral point	M_1	Mission 1 score
α	Angle of attack	M_2	Mission 2 score
δ	Control surface deflection	M_3	Mission 3 score
Units		***Abbreviations***	
A	Amps	AIAA	American Institute of Aeronautics and Astronautics
cm	Centimeter	CA	Cyanoacrylate Adhesive
g	Acceleration under gravity	CAD	Computer-Aided Design
kg	Kilograms	CFD	Computational Fluid Dynamics
m	Meter	CG	Center of gravity
mAh	Milliamp-hours	FEA	Finite Element Analysis
Pa	Pascals	GM	Ground mission
RPM	Revolutions per minute	MAC	Mean aerodynamic chord
s	Seconds	OML	Outer mold line
V	Volts	QADT	Queen's Aerospace Design Team
W	Watts	QAPOT	Queen's Aircraft Performance Optimization Tool
Wh	Watt-hours	RAC	Rated airplane cost
○	Degrees	RFP	Request for proposal
		VLM	Vortex Lattice Method

1 Executive Summary

This report details the design and construction of two fixed wing, carbon fiber planes by QADT's new AIAA division. This report is submitted to participate in the 30th anniversary of the DBF competition, hosted by the AIAA. The team designed two planes, "Tito" and "Turbo" centered around solving the challenges in the DBF RFP which is meant to simulate a banner towing bush plane and charter plane business.

The RFP consists of three flight missions and one ground mission. The first flight mission, M1, is an unloaded, proof-of-flight test, where Turbo must takeoff, complete three laps within five minutes and then successfully land. The second mission is meant to simulate the charter plane side of the business. Turbo must carry rubber ducks and hockey pucks, which simulate passengers and cargo respectively. The goal of this mission is to maximize net income of the make belief business. The final flight mission (M3) simulates the banner towing business. In M3, Turbo must deploy a banner mid-flight and drop it before landing. Once again the objective of this flight is to maximize the business' profit. The ground mission (GM) serves as a design feasibility test. during the GM, a ground crew member, must load and unload all mission payloads as fast as possible.

The team decided designing two planes was the best choice as this is the first year Queen's University has entered the AIAA DBF competition since 2006. The first plane, Tito, serves as a test plane, meant for optimizing manufacturing process and overall design. The second plane, Turbo, will be developed on the knowledge learned through the creation of Tito. Turbo will be the final version of the design and serve as the official competition aircraft.

Both Tito and Turbo feature twin tractor propulsion systems, tapered mid-wing designs, conventional tail and a tricycle landing gear. This overall configuration was chosen primarily because it minimized the chance of interference and instability during the banner mission and it maximized internal space for passengers and cargo. On top of being a test plane, Tito was optimized for manufacturability, where as Turbo was optimized to maximize mission scores by featuring more complex aerodynamic features.

Tito and Turbo share the same construction materials. They both consist of a 2-layer carbon fiber skin and wing spar, with the rest of the structure, including floor, bulk heads and ribs being made of 3mm plywood. This use of carbon fiber on the skin provides a lot of rigidity allowing for a more minimal approach for the internal structure design plane allowing for more passenger and cargo space.

Turbo's predicted mission scores are shown below in Table 1.

Parameter	M1	M2	M3	GM
Predicted Mission Specific Score	1.0	$777.80	440	90s
Predicted Normalized Mission Score	1.0	1.52	2.56	0.5
Total Score	5.58			

Table 1: Predicted Mission Performance

2 Management Summary

2.1 Team Organization

QADT is a student run design team with over 40 years of heritage and experience competing across several Canadian and International competitions. Approximately 160 members spread across 5 different branches, including two technical branches, a business branch in charge of marketing and finance, a research branch, and the Aeroschool branch in charge of coordinating technical and professional development workshops for member development. The QADT AIAA Division is a new technical branch of the team, created to compete in the AIAA DBF Competition for the 2025–2026 school year.

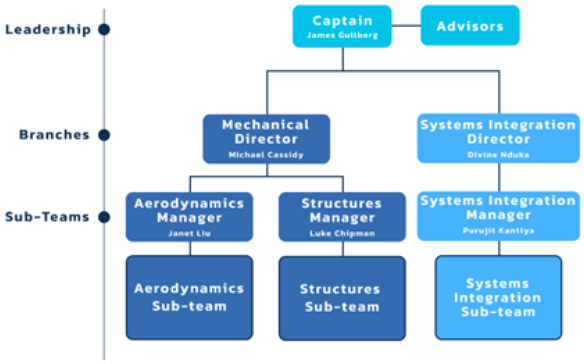

Figure 1: Team management structure.

This new division is led by the AIAA Co-Captain, and is comprised of 3 distinct sub-teams, each consisting of 10 general members from all years and disciplines, led by a manager who coordinates the weekly meetings and ensures a proper distribution of assigned work. Sub-team members work closely with managers as they gain technical skills through hands on work and feedback from the managers. The managers report to directors who are in charge of the administrative tasks, issuing deadlines, ensuring they are met and supporting the managers in technical assignments. The Captain is responsible for facilitating communication between sub-teams and members, while ensuring overarching goal alignment within the team. Faculty and student advisors are available to support the executive team when needed. The team uses this structure to make important technical and managerial decisions. Team leadership meets on a weekly basis to discuss progress updates, timelines, and work together to make decisions with regards to the team's overall direction.

Role	Name	Responsibilities
Aerodynamics	OML design and optimization	CFD, XFLR5, ANSYS
Structures	Airframe design, mold work, fabrication	FEA, CAD, composites
Systems Integration	Avionics, payload, power integration	PCB design, wiring, testing

Table 2: Sub-team responsibilities and skills.

2.2 Schedule

The team's proposed schedule is shown in Figure 2. The executive team has been and will continue to meet weekly to ensure that all tasks and objectives are met in a timely fashion. There is no scheduled work during school breaks to provide a buffer period for any incomplete work. So far in the season, the team has mostly managed to keep up with the timelines. Some adjustments were necessary during the prototype aircraft manufacturing phase.

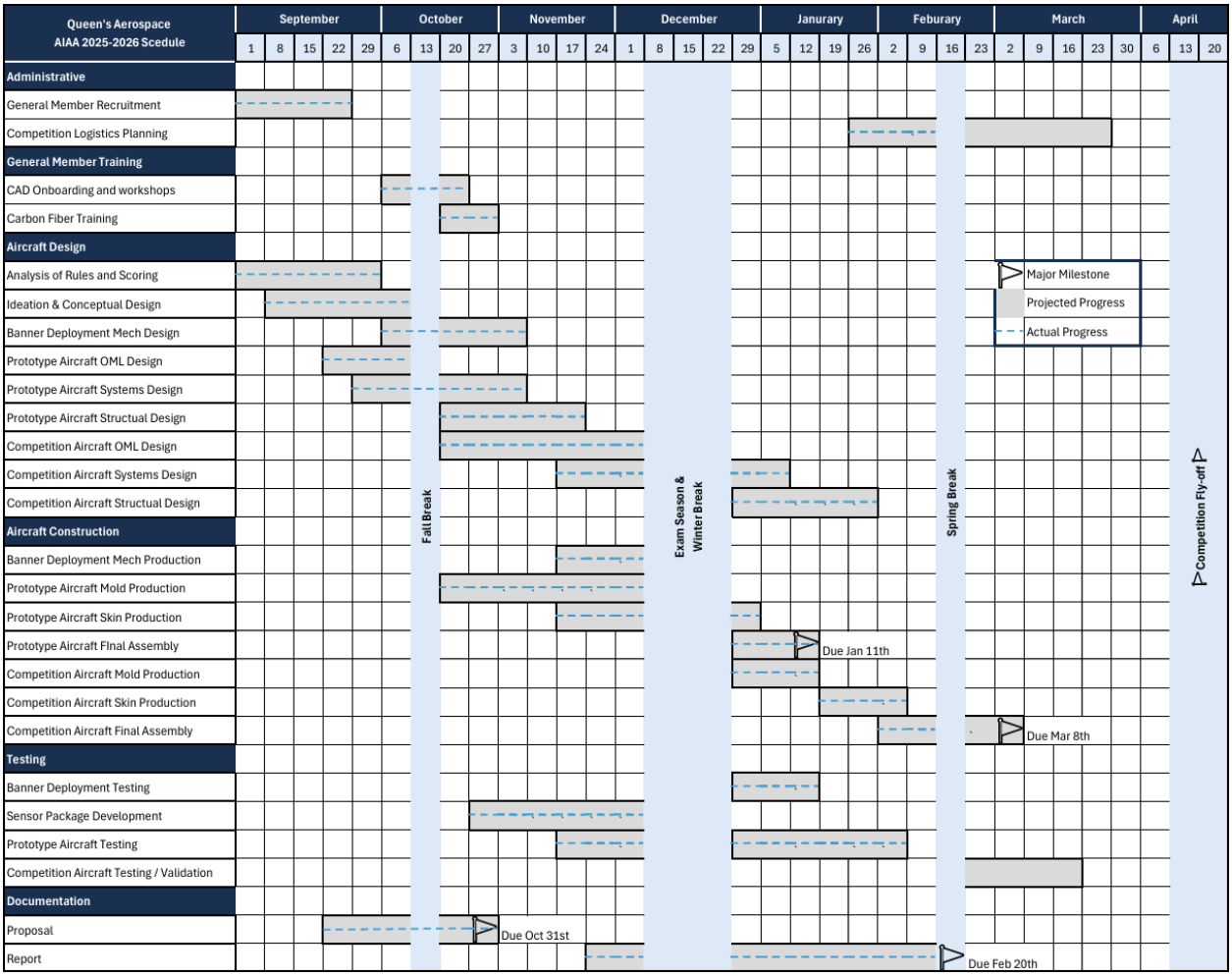

Figure 2: Gantt chart for the 2025-2026 season.

2.3 Budget

The project's total estimated budget for the 2025–26 season is approximately $15,643, with the majority allocated toward travel and competition logistics. QADT has budgeted for 10 members to travel to competition with the team. The team believes that for the future success of the team, it is important that general members gain competition experience and the team plans to subsidize travel to ensure it is accessible. The project will be funded through the Smith Engineering Deans Donation Fund and external sponsorships. Material and fabrication costs remain significant due to the extensive use of composite materials. The team aims to minimize expenses by leveraging in-house manufacturing capabilities and reusing components from previous builds. Some numbers remain estimates as the team is still in process of assembling the competition aircraft and planning travel logistics. However, the exact costs for most items are listed in Table 3. Unless otherwise specified, all costs are listed in Canadian Dollars.

Expenses	Item	Cost
Materials & Fabrication	Carbon Fiber (6oz Twill weave, 50” × 10 YD)	$597
	Layup Material (Vacuum bags, Resin, etc.)	$650
	3D-Printing Filament (PLA and PETG)	$250
	Carbon Tubes and Plywood for internal structure	$350
	Miscellaneous	$220
Electronics Components	Motors (Badass 3515 – 580 KV × 2)	$185
	ESCs (Badass 65 A ESC × 2)	$140
	Rate Gyro (Eagle A3 Rate Gyro)	$50
	Servos (TGY-813 × 5)	$416
	Batteries (Zeee 6S + CNHL 4S LiPo)	$135
Competition Specific Components	Rubber Ducks	$50
	Banner Material (Rip-stop nylon)	$20
	Hockey Pucks	$30
Competition Logistics	Airfare ($850 × 10 members)	$8,500
	Train, Bus, Taxis	$900
	Accommodations ($700 × 3 rooms)	$2,100
	AIAA Membership ($33 USD × 10 = $450 CAD)	$450
	Insurance (Based on prior years spending)	$600
Total		**$15,643**

Table 3: Estimated budget for 2025–26.

3 Conceptual Design

3.1 Problem Statement and High Level Overview

The challenge for the 2025-2026 AIAA DBF competition consists of three phases: the initial design proposal, required for acceptance into the competition, a final design report and the Fly Off, a physical competition that will take place in Wichita, Kansas. The physical competition can further be subdivided into a ground mission and three flight missions which require the team to fly in three configurations: unloaded, with passengers and cargo and with a banner in tow. The overall competition scoring can be seen in Equation (1) and Equation (2) below.

$$M_S = M_1 + M_2 + M_3 + GM \tag{1}$$

$$T_S = (0.15 \cdot P_S \cdot M_S) + (0.85 \cdot R_S \cdot M_S) \tag{2}$$

3.2 Staging and Mission Specifications

At the AIAA DBF fly off, the team will need to complete the three flight missions in order. Before each mission, the team is allowed a 5-minute staging period to prepare for the upcoming flight. This includes checking flight controls, installing propulsion batteries, payloads, and the banner which may not be prepared beforehand. All the assembly work on the plane must be performed in its upright position by a designated ground crew member.

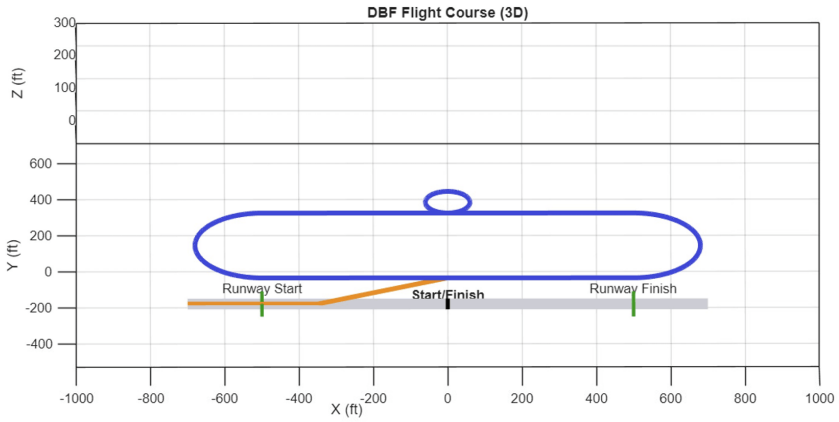

Figure 3: 3D course model made in MATLAB.

After the staging period, the declared mission will be flown on the official flight course. There is a 5-minute flight window starting from when throttle is first applied and ending when the plane crosses the start/finish line prior to the landing lap. A 3D model of the flight course created in MATLAB is shown in Figure 3. The flight course consists of two straights; two 180 degree turns and one 360 degree turn. The mission starts with a rolling takeoff in the upwind direction, followed by the first 180 degree turn into the downwind direction. During the downwind straight, the plane must perform a clockwise 360 degree turn. At the end of the downwind straight the second 180 degree turn must be performed back into the upwind direction. The lap is completed when the plane once again passes the start/fin line. Each straight segment is 1000 ft long. The length of each turn is dependent on the turning radius of the plane. Assuming a turning radius of roughly 10.5 m, the total distance per lap is 742 m.

3.3 Mission 1 Description and Scoring

M1 requires the team to complete three laps within the 5-minute flight window and successfully land. This mission should be flown in the unloaded configuration (no payload). This mission is pass/fail; one point is awarded for a successful flight. Scoring is shown in Equation (3).

$$M_1 = 1.0 \tag{3}$$

3.4 Mission 1 Design Requirements Analysis

The initial ground roll is estimated at 10 s, and an additional 10 s is allocated to the upwind climb into the first lap. This leaves 280 s to fulfill lap times (93 s/lap). This correlates to a minimum cruise speed of approximately 8.1 m/s. The aircraft must be maneuverable enough to complete the turns required in the lap.

Label	Subsystem	Requirement
M1-1	Propulsion	The plane must have a high enough cruise speed to complete three laps within 5 minutes.
M1-2	Structures	The plane must withstand the maximum predicted loads of unloaded takeoff and landing.
M1-3	Aerodynamics	The plane must have a low enough turning radius to complete the required maneuvers.

Table 4: M1 design requirements.

3.5 Mission 2 Description and Scoring

M2 is meant to simulate a charter flight business being operated using the team's plane. Standard rubber ducks are used in place of human passengers and hockey pucks are used as cargo. The team must load the plane with at least three passengers and one piece of cargo. In this mission the team must maximize income while minimizing costs, these are calculated using Equation (5) and Equation (6), respectively. The scoring consists of a fixed one-point completion point and up to one additional point based on the team's net income compared with that of the competition leader. The variables which affect the team's score in this mission are the amount of cargo and passengers on the plane during flight, the number of laps completed within the flight window, and the efficiency factor. The efficiency factor is calculated by dividing the battery capacity by 100, incentivizing a power efficient design. The total M2 score can be calculated with Equation (4).

$$M2 = 1 + \frac{\text{NetIncome}_{\text{Team}}}{\text{NetIncome}_{\text{Max}}} \tag{4}$$

$$\text{Income} = CC_p \cdot (\text{Ip1} + (\text{Ip2} * L_2)) + CC_c \cdot (\text{Ic1} + (\text{Ic2} * L_2)) \tag{5}$$

$$\text{Cost} = L_2 \cdot (C_e + (CC_p \cdot C_p) + (CC_c \cdot C_c)) \cdot E_f \tag{6}$$

3.6 Mission 2 Design Requirements Analysis

For M2, requirements arise from the mission payload. There must be enough space within the plane to house the passengers and cargo. Additionally, the cargo, passengers and avionic/propulsion systems must be physically separated within the plane with a bulkhead. Apart from space requirements, the plane must generate enough lift and have greater control authority to support the additional load. Finally, the plane must have hatches to load and unload the payload for this mission. A detailed list of requirements is shown in Table 5.

Label	Subsystem	Requirement
M2-1	Structures	The plane must be capable of carrying a minimum of three passengers.
M2-2	Structures	The plane must be capable of carrying a minimum of one cargo.
M2-3	Structures	The plane must have a single passenger compartment.
M2-4	Structures	The plane must carry at least three passenger per piece of cargo.
M2-5	Structures	The passengers must be situated on a single plane which is parallel to the horizontal plane while in flight.
M2-6	Structures	The passenger compartment must be accessed by one or more hatches in the plane.
M2-7	Structures	The passenger door must only provide access to the passenger compartment.
M2-8	Structures	Cargo must be stored in one or more bays in the plane.

Label	Subsystem	Requirement
M2-9	Structures	Each cargo bay must have exactly one door.
M2-10	Structures	The passengers must board the plane individually.
M2-11	Structures	The passengers must sit in an upright position and remain fixed during flight.
M2-12	Structures	Cargo must be restrained during flight to prevent movement.
M2-13	Aerodynamics	The plane must have enough stability to overcome changes in CG and total mass from the passengers and cargo.
M2-14	Aerodynamics	The plane must have enough yaw authority to have a reasonable turning radius with the added inertia of the payload.

Table 5: M2 design requirements.

3.7 Mission 3 Description and Scoring

For M3, the plane must deploy a banner mid-flight, fly as many laps as possible within the 5-minute flight window, then drop the banner before landing. The mission score is determined by the length of the banner, the number of laps flown and RAC. The RAC is a linear function of the aircraft wingspan, calculated using Equation (7), which negatively impacts the M3 score (i.e. RAC should be minimized). Additionally, there is a two-point completion bonus for all teams that successfully perform the mission. The M3 score can be calulated using Equation (8).

$$RAC = \frac{0.05 \cdot WS}{12} + 0.75 \tag{7}$$

$$M_3 = \frac{L_3 \cdot B_L}{RAC} \tag{8}$$

3.8 Mission 3 Design Requirements Analysis

Three structural requirements arise from this mission. First, the banner must be stowed externally to the plane for the first portion of the flight. Second, a mechanical subsystem must deploy the banner mid-flight and tow it behind the plane such that it is held vertically. Finally, the banner must be released by the plane before landing in such a way that the banner is not damaged. There are also some aerodynamic design considerations that arise from this challenge. The plane must be passively stable to ensure the unpredictable nature of the banner does not impede performance during all phases of the flight. The plane must also generate enough lift and thrust to overcome the added weight and drag of the banner in-flight. Finally, the plane must be configured such that the banner does not get caught on any features of the skin while being deployed or after release. A full list of M3 requirments is shown in Table 6.

Label	Subsystem	Requirement
M3-1	Structures	The plane must stow the banner externally.
M3-2	Structures	The banner cannot interfere with flight or control functions.
M3-3	Systems Integration	The banner must be deployed and released remotely.
M3-4	Structures	The banner must remain vertical once deployed.
M3-5	Aerodynamics	The plane must be capable of dealing with the added loading an instability of towing the banner.
M3-6	Structures	The banner mut not be damaged during any phase of the deployment/release process.

Table 6: M3 design requirements.

3.9 Ground Mission Description and Scoring

The GM requires the team to set the plane up in the M2 and M3 configurations as quickly as possible while in its upright position (i.e. on landing gear). In phase one, the plane starts unloaded and then a member of the team must load all the passengers and cargo into the plane. In the second phase, the same team member must unload the passengers and cargo and install the banner. Finally, the team member must lift the plane so it is pointing upward and show that the banner can be deployed and released from the plane. There is no completion points for this mission. The team can score up to one point based on their completion time compared to that of the competition leader. The GM score can be calculated using Equation (9).

$$G_M = \frac{\text{Time}_{\text{Team}}}{\text{Time}_{\text{Max}}} \tag{9}$$

3.10 Ground Mission Design Requirements Analysis

The main design consideration for the ground mission is the configuration of the access hatches on the plane. In order to minimize loading time, cargo, passenger and electronic hatches must be easily accessible to the ground crew member when the plane is in its upright position. Similarly, the banner release mechanism should allow for the banner to be easily installed during the ground mission. The banner must also be deployable under the force of gravity for the demonstration segment of the ground mission. A list of all GM design requirements is shown in Table 7.

Label	Subsystem	Requirement
GM-1	Structures	All hatches for passengers and cargo must be accessible with the airplane sitting on the landing gear.
GM-2	Structures	The loading and unloading method for the passengers and cargo must be repeatable and minimally complex to perform.
GM-3	Structures	The banner must be deployable under the force of gravity.
GM-4	Structures	The loading and unloading method for the banner must be repeatable and minimally complex to perform.

Table 7: GM design requirements.

3.11 Non-mission Based Requirements

As a part of the AIAA DBF rule book, there are several requirements imposed upon designs for safety, logistical and competitive reason. These requirements do not fall under a specific mission, but are none the

less important to consider when designing the plane. All non-mission based requirements are summarized in 8. Additionally, Table 9 outlines absolute design constraints on the planes configuration.

Label	Subsystem	Requirement
S-1	Structures	Door hatches must be rigidly attached when opening and in the open configuration.
S-2	Aerodynamics	The airplane must have the loaded and unloaded CG locations marked on the exterior.
S-3	Structures	No structure may be dropped from the plane during flight, unless required by a mission objective.
S-4	Structures	Structures, components and payloads must be mechanically fastened and cannot use friction as their primary retention method.
S-5	Systems Integration	All energy for the flight must come from on-board propulsion battery pack(s).
S-6	Systems Integration	Propellors must be driven by an over the counter, unmodified brushed or brushless electric motor.
S-7	Systems Integration	The airplane must be manually controlled by radio by a pilot with only rate gyros as electronic control systems.
S-8	Aerodynamics + Systems Integration	The airplane must use commercially available propellors with limited modification.
S-9	Structures	The takeoff gross weight with payload must be less than 55-lb.
S-10	Systems Integration	The airplane must have an externally accessible switch to turn on the radio control system.
S-11	Structures	Components secured with fasteners must use secondary retention methods.
S-12	Structures	All aerodynamic components must resist aeroelastic effects.
S-13	Structures	Motors and propellors must be adequately secured to the plane to resist all expected loads.
S-14	Systems Integration	All electrical connections must be fully insulated.
S-15	Systems Integration	The airplane must have a blade style mechanical motor arming fuse for each propulsion system.
S-16	Structures + Systems Integration	The arming fuse must be located externally on the plane such that a crew member does not need to reach over the propellor to access it and it must not be within 6 inches of the propellor.
S-17	Systems Integration	All battery packs must be un-altered and commercially procured as Commercial-Off-The-Shelf (COTS) battery packs.
S-18	Systems Integration	A separate battery is required for the Rx/Servo battery on the airplane. There is no restriction on the Rx/Servo and Transmitter battery type regardless of the propulsion battery type.
S-19	Systems Integration	All propulsion battery packs must be identical.
S-20	Systems Integration	Each battery pack must be independently connected to its own propulsion system.

Label	Subsystem	Requirement
S-21	Systems Integration	Each battery/propulsion system is required to have its own Arming Fuse.
S-22	Systems Integration	The maximum current rating for the arming fuse is the maximum continuous discharge current rating of the battery pack (battery capacity multiplied by C-rating or maximum labeled discharge current) up to 100 amps.

Table 8: Competition safety, logistical and systems requirements.

Label	Subsystem	Requirement
C-1	Aerodynamics	Wingspan must be less than 5 feet.
C-2	Aerodynamics	The plane must not use rotary wings or lighter-than-air configuration.
C-3	All	The airplane must be capable of performing all missions.
C-4	Structures	The airplane must be capable of passing a wingtip loading test in its heaviest configuration.
C-5	Aerodynamics	The airplane must be capable of dealing with the added loads of towing a banner of a minimum length of 10 inches and an aspect ratio of 5.
C-6	Systems Integration	Total Propulsion Energy stored on airplane (sum of all propulsion batteries) shall not exceed 100 Watt-hours.

Table 9: Competition plane configuration constraints.

3.12 Scoring Sensitivity Analysis

Figure 4 shows a sensitivity analysis for M2. There are three main parameters when it comes to determining M2 score. First is the carrying capacity of the plane, which determines the net income per lap. The net income per lap is calculated using Equation (5) where 5 laps are used as a reasonable baseline. The second graph in the figure shows the effect of battery cost on M2 score. The battery cost affects the score through the EF in cost as shown in Equation (6). The third graph shows the effect of the number of laps flown on M2 score. The graphs indicate that net income (passenger and cargo capacity) and laps flown are far more important than the battery cost and therefore a successful design for M2 will prioritize these aspects.

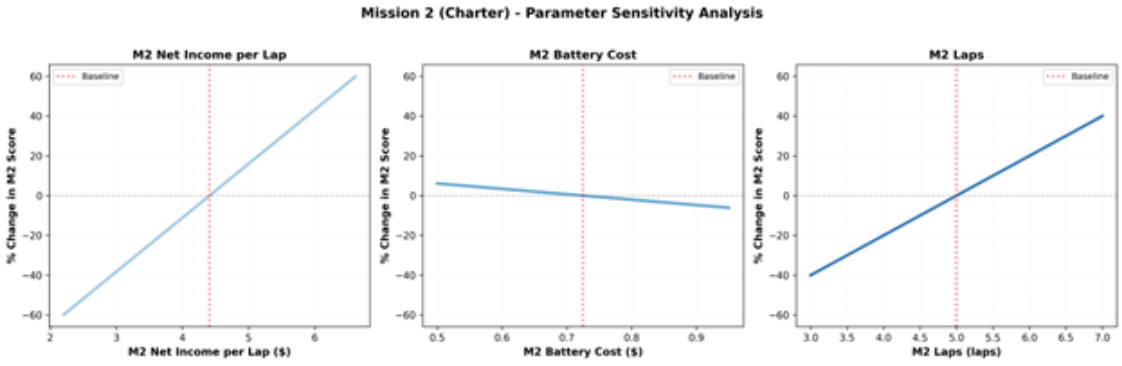

Figure 4: Scoring sensitivity analysis for M2

For M3 scoring there are once again three major contributing parameters. The first is the number of laps completed in the flight window. Second, is the length of the banner being towed and the third is the wingspan of the plane. All of the parameters contribute linearly to the score, but since the wingspan value is scaled, it contributes significantly less to the overall score. A successful design for M3 will prioritize increasing banner length and increasing the number of laps flown.

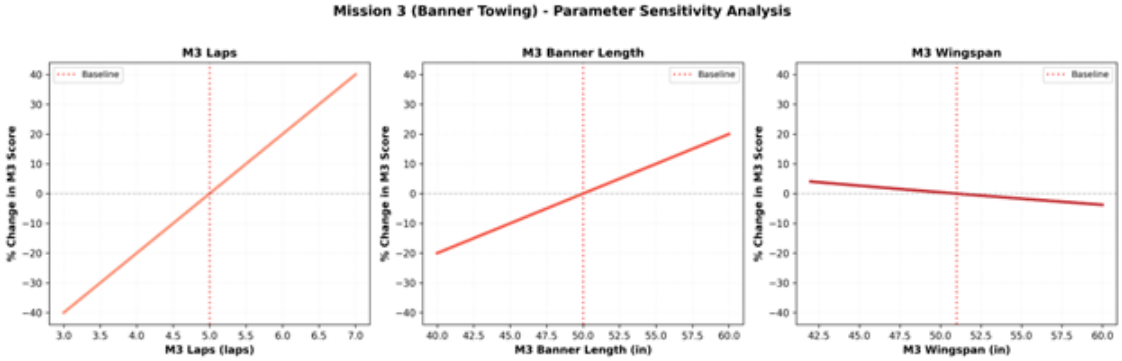

Figure 5: Scoring sensitivity analysis for M3

The sensitivity analysis revealed a set of key parameters that must be prioritized. To maximize mission scores, the team has prioritized a design optimized for a high volume of laps within the flight window, high passenger and cargo capacity and large banner size. Prioritizing these parameters comes at the cost of optimized battery capacity and wingspan.

When selecting the configuration of the plane manufacturability, flight speed, maneuverability and stability were heavily weighted. Manufacturability is an important parameter because creating an easily manufacturable design increases the likelihood of meeting deadlines and successfully producing the airplane. Flight speed and maneuverability are considered since they both contribute to maximizing laps flown within the flight window. Finally, Stability is an important parameter because it will allow the airplane to tow a large banner without losing control.

3.13 Configuration Selection

Key characteristics of the plane are determined by conducting a trade study through Figure of Merit (FOM) charts. Based on the sensitivity analysis and team goals, performance metrics are given a weighted value. Each metric is assessed between 0 and 1 according to basic flight characteristics and team experience with manufacturing.

3.13.1 Wing Shape

To determine the general configuration, biplane, monoplane, and flying wing configurations were considered. Subsequently, the decision to include taper or have rectangular wings was considered. Stability ruled out a flying wing configuration, while payload loading compatibility and manufacturability ruled out the biplane configuration. Therefore, a monoplane configuration was decided upon. Taper and rectangular wings scored qualitatively similar as there are no advantages to taper at low speeds. Ultimately, taper was decided upon due to its structural advantage since the main support bar goes through the $\frac{1}{4}$ point. The scoring is detailed in Table 10.

						
Figures of Merit	**Factor**	**Biplane**	**Monoplane**	**Flying Wing**	**Taper**	**Rectangular**
Manufacturability	0.3	0	1	0	1	0.8
Stability	0.3	0.7	1	0.3	1	1
Maneuverability	0.1	0.8	1	0.8	1	1
Flight Speed	0.2	0.5	1	0.4	1	1
Payload Loading Speed	0.1	0	0.8	0.5	1	1
Total		**0.39**	**0.98**	**0.3**	**1**	**0.94**

Table 10: Wing shape figures of merit

3.13.2 Tail and Wing Placement

Wing placements are evaluated based on manufacturability, aircraft control, and payload compatibility. A low–wing was ruled out for instability and manufacturing difficulty. A high-wing offers the most stability control and compatibility with cargo loading, however the team's priority was ease of manufacturing. A mid-wing allows for a simpler seam line for the carbon fiber molds, and for this reason, a mid-wing was decided upon. For tail configurations, a T-tail was ruled out for lack of manufacturability. The conventional and V-tailed scored similarly. While the team has more experience manufacturing V-tails and the V-tail configuration has the potential to minimize weight, ultimately a conventional tail was decided upon for its reliability and abundant online documentation. The scoring is detailed in Table 11.

							
Figures of Merit	**Factor**	**High-Wing**	**Mid-Wing**	**Low-Wing**	**T-Tail**	**Conventional Tail**	**V-Tail**
Manufacturability	0.4	0.5	0.9	0.2	0.5	0.89	1
Stability	0.3	0.9	0.7	0.3	0.8	1	0.9
Maneuverability	0.2	0.7	0.8	0.9	1	1	0.9
Payload and Banner Compatibility	0.1	0.7	0.6	0.7	1	0.9	0.9
Total		**0.68**	**0.79**	**0.42**	**0.74**	**0.95**	**0.94**

Table 11: Wing placement figures of merit

3.13.3 Propulsion and Landing Gear Configuration

The propulsion system was evaluated across tractor, pusher, and twin-engine configurations. A primary design driver was payload integration, specifically regarding banner compatibility and the associated interference risks. To eliminate the possibility of the banner tangling with the propulsion system, which is a significant hazard in pusher layouts, a tractor configuration was prioritized. There is no take-off distance limit for the missions; however, the take-off time is part of the mission time limit. From the sensitivity analysis, the team is prioritizing total laps over battery capacity. The single tractor offers lighter weight and lower power consumption. However, due to the climb-out time, a twin configuration was decided upon to increase thrust

availability and ultimately climb speed even though it draws more power and would require a larger battery capacity.

For landing gear configuration, only a tricycle and taildragger were considered. The tricycle configuration has significantly better handling characteristics on the ground. Additionally, the taildragger poses an interference risk to the banner attachment mechanism. For these reasons, a tricycle configuration was decided upon. The scoring is detailed in Table 12.

						
Figures of Merit	**Factor**	**Tractor**	**Pusher**	**Twin**	**Tricycle**	**Taildragger**
Stability	0.1	1	1	1	1	0.8
Weight	0.3	1	1	0.8	1	1
Component, Payload, Banner Compatibility	0.5	0.9	0	1	1	0.5
Thrust	0.1	0.7	0.6	1	–	–
Total		**0.92**	**0.46**	**0.94**	**0.9**	**0.63**

Table 12: Propulsion and landing gear figures of merit

3.13.4 Final Conceptual Design

The first concept of the design is a mid-wing, tricycle gear, monoplane with a conventional tail and twin propulsion system. It is designed to be stable, cargo and passenger compatible, and able to support a banner deployment mechanism attached to the underside of the empennage.

4 Preliminary Design

4.1 Design Process and Analysis

4.1.1 Design Methodology

The team decided to take a two iteration design approach. The plan was to create two planes, where the first version (Tito) would be a proof of concept to test the team's design/manufacturing approach. For the second plane (Turbo), lessons learned from the creation of Tito would be applied to ensure a viable and competitive aircraft was brought to the fly off. Below, only the design methodology followed for the first iteration is described, but the exact same steps are repeated for iteration 2.

The first step in the design process was to understand the RFP and to define the problem. The team spent time understanding and interpreting the rules and mission requirements to derive all functional requirements for the plane. The results of this process are outlined in Sections 3.1 to 3.11. From this analysis, the team found several competing variables that play an important role in the mission scores. A sensitivity analysis was performed on the scoring equations to gain an understanding of which variables were heavily weighted in the score. Guided by the results of the sensitivity analysis, the team identified the most important factors to consider when selecting a configuration for Tito. Several high level designs were compared using weighted

evaluation matrices, with scores assigned to each design based on their alignment with the team's design priorities. Once a configuration was selected, the aerodynamics sub-team started Tito's preliminary design with close collaboration with the systems integration sub-team for appropriate propulsion system sizing. QADT's OML design process is centered around repeated iteration using OpenVSP and QAPOT to optimize the geometry of the plane. This process also includes performing trade studies on the different aspects of the design. The exact aerodynamic design process is documented in Sections 4.1.2 to 4.3.4.

Once the OML design was completed it was passed on to the structures sub-team to begin the manufacturing process. While manufacturing was under way, the aerodynamics team continued to analyze Tito's design using CFD tools before beginning work on Turbo. The manufacturing process began with selecting materials and manufacturing methods. Weighted evaluation matrices were used to ensure that each material/method was equally considered. In the end, it was determined that the best structural design would make use of a carbon fiber shell that would be created in house and a CNC cut internal strcuture. The complete structures design process is documented in Section 6.

Once the structure was manufactured, the systems integration and structures sub-teams worked together to assemble the plane. During this phase, the aerodynamics and systems integration sub-team also began system testing to collect data that can be used to improve Turbo's design. The design methodology outlined will also be used for the design and development of Turbo, including data collection for iteration/improvement.

4.1.2 Design Trades Studies

The team completed a prototype plane since this is the first time QADT has competed in DBF since 2006 and faces many uncertainties. Unless specified, all information is for Turbo. Tito is intended to have a quick design turnover to confirm basic aerodynamic concepts, manufacturing processes, and ensure a plane is available for testing banner mechanisms. Between Tito and Turbo, further research, stability and CFD analysis was conducted to inform the final design.

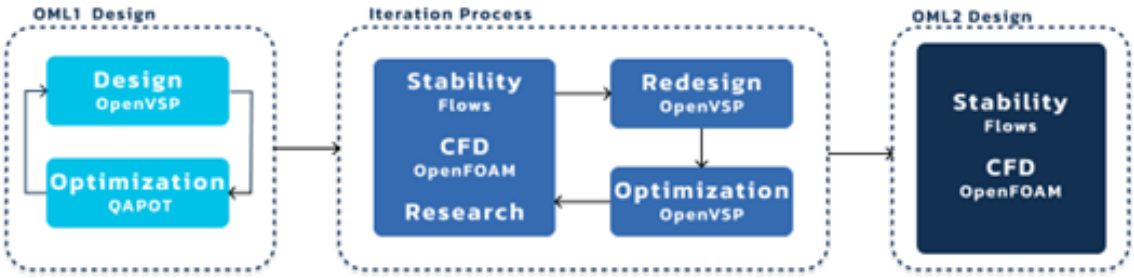

Figure 6: Aerodynamic design process flow chart.

4.1.3 General

The team has a custom Python optimization script using the AeroSandBox library called Queen's Aircraft Performance Optimization Tool (QAPOT). An initial plane design is created in OpenVSP and the parasitic drag coefficients are inputted into QAPOT. The material densities and the scoring equation for M2 are defined in QAPOT, and the optimization goal is set to maximize the M2 score. QAPOT outputs the optimized design parameters such as wingspan, chord length, tail span and it's chord length. It also outputs predicted

performance such as cruise speed, stall speed, endurance, and predicted score. QAPOT is used as a starting point; detailed design parameters and performance are established later.

4.1.4 Empennage Sizing

Based on the results of the sensitivity analysis, the preliminary design used the maximum wingspan. QAPOT was used to optimize areas and volumes, and their respective coefficients were used as a guideline in further iterations. The final values are shown in Table 13. These coefficients were finalized using evidence from literature and team experience in other design competitions.

Component	Area/Volume	Coefficient
Wing	0.510 m^2	
Horizontal Stabilizer	0.436 m^3	0.397
Vertical Stabilizer	0.027 m^3	0.025

Table 13: Empennage sizing table.

4.1.5 Airfoil Selection

Airfoil evaluation and selection was conducted to ensure reliable aerodynamic performance across the entire expected operating envelope while remaining compatible with team manufacturing ability. Based on estimated performance figures, the aircraft is expected to operate mainly within the Reynolds number range of 300,000 to 550,000 with an estimated cruise condition of $Re = 530,000$.

To better evaluate airfoil performance the required lift coefficient at cruise was estimated using Equation (11),

$$C_L = \frac{L}{\frac{1}{2} \cdot \rho \cdot V^2 \cdot S} \tag{10}$$

where L was set equal to aircraft weight, V to expected cruise velocity, S calculated based on wing geometry, and ρ estimated in accordance with expected conditions. The resulting lift coefficient at cruise was found to be approximately 0.25. This value was used as an evaluation point for determining airfoil efficiency at cruise flight.

Various candidate airfoils typically used for low to moderate Reynolds number operation were chosen for preliminary evaluation. Using the Airfoil Tools website (accessed 2026), the initial candidate airfoils were narrowed down to five contenders: AG16, Clark-Y, NACA 2412, N10, and S7055. To assess these airfoils various polars such as coefficient of lift vs angle of attack and coefficient of drag vs coefficient of lift were generated using Flow5 software seen below in Figure 7.

To objectively compare the airfoils a weighted evaluation matrix was created that evaluates each airfoil's performance across criteria defined as most critical to mission success. As seen in Table 14 each criterion was assigned a weight factor based on its relative importance to the mission. This led to metrics such as max lift coefficient and cruise lift to drag ratio contributing more to the airfoils final valuation. Scores were awarded based on aerodynamic performance evaluated at critical values such as cruise C_l of 0.28 and through consulting the structural sub-team for evaluation on the mannufacturability metric.

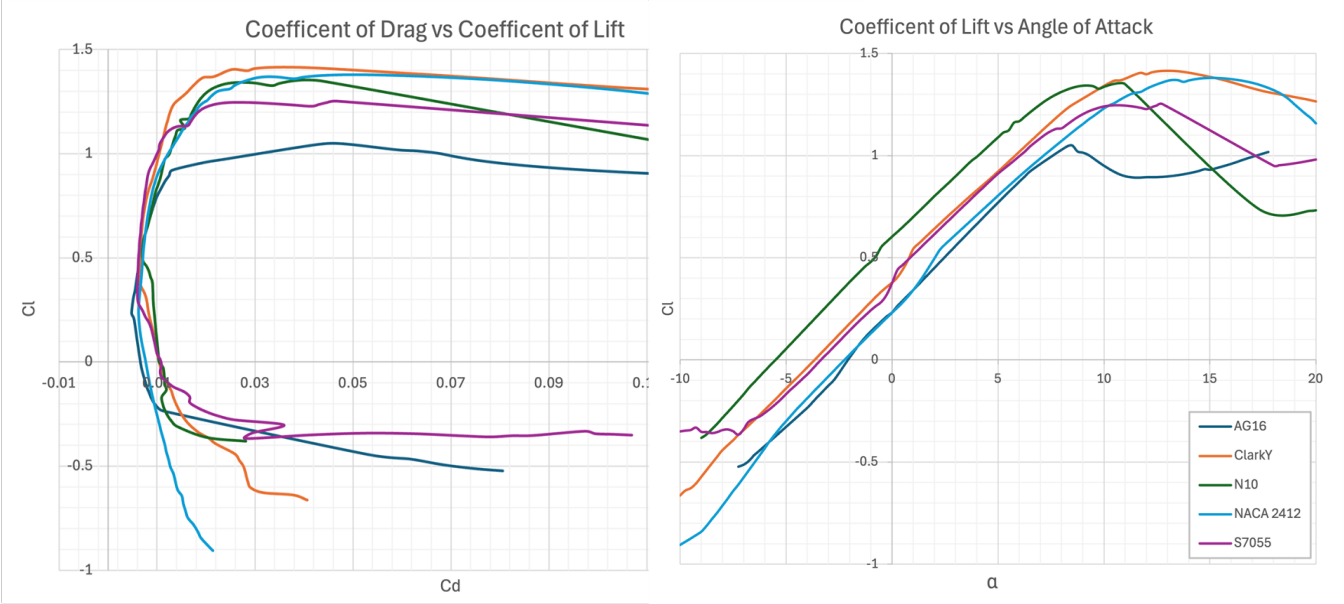

Figure 7: Coefficient of Lift vs Angle of Attack (Left) and Coefficient of Drag v. Coefficient of Lift at Cruise Re of 530,000 (Right)

Characteristic	Factor	AG16	Clark-Y	N10	NACA2412	s7055
Maximum Cl	0.3	1	5	4	4	3
Cruise L/D	0.25	5	4	4	4	5
Operating Envelope (stall)	0.25	2	5	3	5	3
Manufacturability	0.2	2	4	5	3	3
	1	**2.45**	**4.55**	**3.95**	**4.05**	**3.5**

Table 14: Weighted evaluation matrix of the top 5 performing airfoils.

From the weighted evaluation matrix, it was determined that the best airfoil for the mission was the Clark-Y airfoil, which achieved the highest overall score. Although other airfoils demonstrated better cruise lift to drag ratio and manufacturability, the Clark-Y maintained a favorable performance across the board. It especially excelled in the operating envelope category, which served as the main reason to switch from the N10 used in preliminary designs. The Clark-Y airfoil exhibits great max lift, efficient cruise flight, and has a relatively thick, flat-bottomed geometry making it the best overall choice for the aircraft.

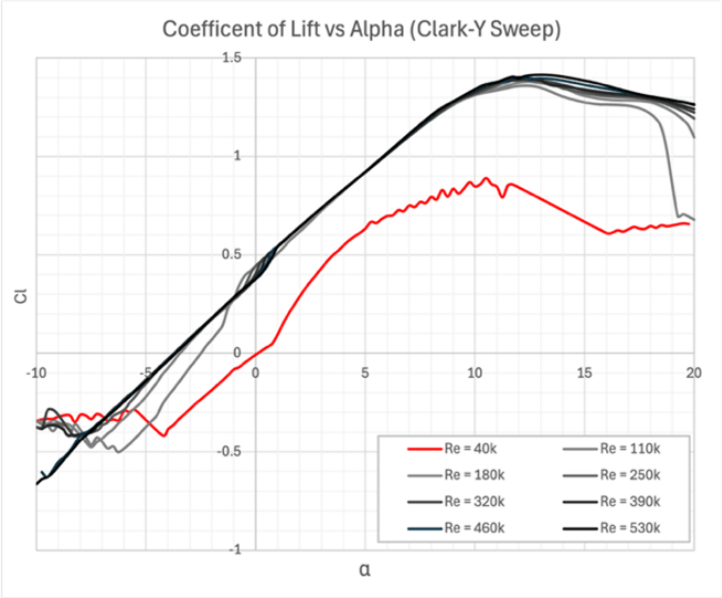

Figure 8: Coefficient of Lift vs Alpha Clark-Y Re Sensitivity Sweep.

To further assess the Clark-Y's mission compatibility, a Reynolds number sensitivity analysis was performed evaluating the airfoil over a sweep of Re values from 40,000 to 530,000 in flow5. Results of this analysis are shown in Figure 8. The results demonstrated a consistent lift curve with no abrupt loss in performance until a Re of 40,000 was reached. However, a Re of 40,000 is far outside the expected operating range, confirming that the Clark-Y airfoil will perform reliably and predictably across the relevant Re range.

Overall, based on its score in the weighted evaluation matrix and consistent behavior across a wide range of Re values, the Clark-Y airfoil was selected for the final wing design.

4.1.6 Banner and Drag Analysis

The aircraft and banner were modeled in OpenVSP to determine drag contributions and parasitic drag coefficients. The banner deployment mechanism and landing gears are neglected. The zero lift drag contributions are shown in Figure 9. The total parasitic drag coefficients are 0.02144 and 0.02763 for M1/M2 and M3 respectively. The main drag contributors were wing profile drag for all missions and the banner for M3. During the iteration phase, reducing wing drag was a priority and is detailed in Section 4.1.7. Banner drag impact is detailed in Section 4.2.5.

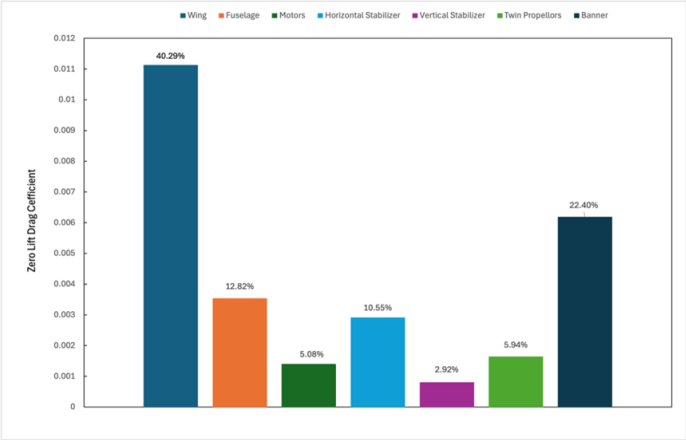

Figure 9: Zero lift drag coefficient contributions.

Banner Parameter	Value
Length	55 in
Width	11 in
Total Mass	64 g

Table 15: Banner Parameters

4.1.7 Wing and Control Surfaces

The aircraft wing was qualitatively analyzed from the initial QAPOT starting point, Tito. Changes are verified quantitively using flow5. Both Tito and Turbo have a maximized wingspan and a taper of 0.6; a taper of 0.7 was analyzed in flow5 and was determined to be slightly less efficient.

Parameter	Tito	Turbo
Span	1.5 m	1.5 m
Area	0.56 m^2	0.51 m^2
Aspect Ratio	3.98	4.4
Root Chord	0.47 m	0.43 m
Tip Chord	0.28 m	0.26 m
Taper	0.60	0.60
Sweep	0.25	0.25
Dihedral	1.5°	3°
Root Twist	0°	0°
Tip Twist	0°	-2°
Airfoils	N-10	Clark Y

Table 16: Wing Geometry Comparison Between Tito and Turbo

Wing twist for Turbo is 2 degrees of washout, reducing angle of attack from root to tip. Washout causes the root to stall first while wingtips remain at lower angles of attack [1], preserving aileron effectiveness and roll authority at low speeds. In high-bank turns, down-going ailerons can locally induce tip stall and wing drop; washout prevents this by keeping tips farther from stall. It also reduces wingtip vortex strength and drag at high angles of attack, improving yaw stability and rudder effectiveness, [1]. The 2-degree washout ensures predictable stall progression.

Wing dihedral provides roll stability at low airspeeds. When the aircraft rolls or sideslips, angle of attack increases on the lower wing, creating a restoring moment back to level flight, [2]. Turbo has 3 degrees of dihedral for reliable lateral stability without excessive roll stiffness.

Wing taper ratio (tip chord to root chord) determines lift distribution and influences induced drag and stall behavior. Lower taper ratios produce higher wingtip lift coefficients, increasing tip stall susceptibility and roll control loss, [3]. Higher ratios shift maximum lift inward, improving stability. The effect on efficiency is non-linear, [3]: small ratios reduce induced drag but worsen stall; large ratios increase induced drag and reduce Oswald efficiency. Turbo's taper ratio of 0.60 balances low-speed handling with efficiency.

Wing sweep provides minimal aerodynamic benefit at low speeds and reduces lift coefficient, [4]. For Turbo, sweep is a manufacturing consideration. The wing uses sweep at quarter-chord to simplify construction and maintain lift efficiency.

For control surfaces, the aircraft has ailerons, an elevator, and a rudder. Tito was intended to have flaps but was not implemented due to manufacturing delays and analysis which showed sufficient lift from the wings. The control surfaces were evaluated using past team designs and other DBF competition specs. The aileron, elevator, and rudder have chords 30%, 40%, and 50% respectively with a span limited by structural considerations. The maximum deflection for the aileron, elevator, and rudder is 30, 45, and 45

degrees, respectively. Control surface authority is verified during flight testing.

4.1.8 Preliminary Specifications

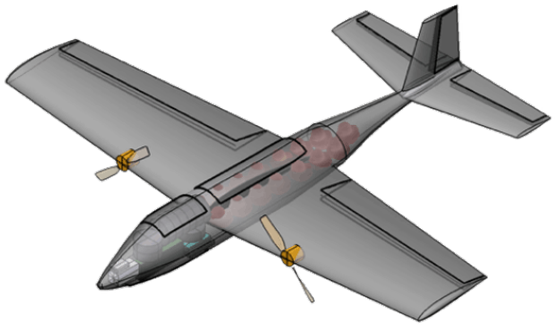

Figure 10: Final Turbo OML design.

Following the iteration process, Turbo was finalized in OpenVSP and is shown in Figure 10. A preliminary weight estimate of 4.24 kg was used in performance evaluation. Table 17 shows select variables and parameters used in QAPOT to finalize the design.

Parameter	Value
ρ – Air Density	$1.225\ kg/m^3$
e – Oswald efficiency factor	0.80
k – Induced drag factor $= \frac{1}{\pi ARe}$	0.0904
g – Gravitational acceleration	$9.81\ m/s^2$
Wing Reference Area	$0.510\ m^2$
AR	4.40
m – Aircraft mass	$4.24\ kg$
W – Aircraft weight $= mg$	$41.59\ N$
T – Takeoff thrust	$24.29\ N$
$C_{L_{\text{max}}}$ – Maximum Lift Coefficient	1.4152
$C_{D,0}$ – Zero lift drag coefficient (M1,2 and M3 avg.)	0.0245

Table 17: Select Parameter Values

4.2 Aircraft Performance

4.2.1 Overall Lift and Drag

During initial optimization using QAPOT, an Oswalds efficiency factor of $e = 0.80$ was used based on past designs. The selected airfoil is simulated using XFoil through flow5 under M2 conditions to determine stall angle and maximum lift coefficient. The simulation revealed stall angle of 13° and maximum lift coefficient of 1.4152. In the final analysis, the coefficients and forces the aircraft is subject to are determined using flow5 under the M1 conditions and weight equaling lift. The values are summarized in Figure 11 and Figure 12. Flow5 data is used for most analysis, however, since it is a VLM, the airfoil data was transformed from 2D to 3D using Equation (11) to determine the 3D stall angle. The final stall angle and stall speed were found

to be 13° and 9.60 m/s respectively.

$$C_{L,3D} = \frac{C_L}{1 + \frac{C_L}{\pi e A R}} \tag{11}$$

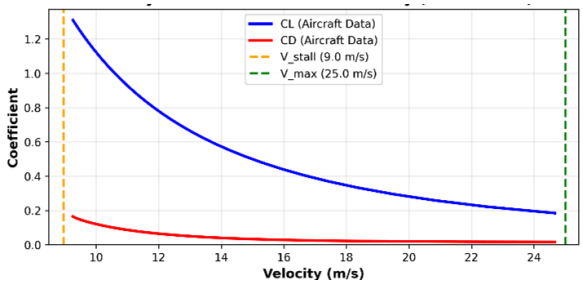

Figure 11: Lift and Drag Coefficients vs Velocity

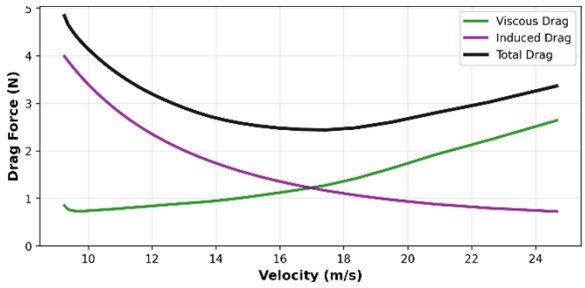

Figure 12: Drag Components vs Velocity

4.2.2 Maneuverability

Various maneuvers were analyzed to ensure adequate performance, prevent stall and minimize structural damage. Relevant maneuver parameters include the load factor, bank angle, turn rate and turn radius. The load factor for an airplane is defined as the aerodynamic stress on the structure and is expressed in G-forces. In a straight level flight, the load factor is 1 G. The load factor is found from Equation (12).

$$n = \frac{L}{W} \tag{12}$$

where n is the load factor, L is the lift, and W is the weight. In a balanced turn, the load factor is defined by Equation (13).

$$n = \frac{1}{\cos\theta} \tag{13}$$

where θ is the bank angle. For the load factor, the lift is the overall lift provided by the wing, fuselage and tailplane, not purely the aircraft's wing. From Equation (13), a maximum bank angle was used in order to determine turn radius and angular velocity, found using Equation (14) and Equation (15), respectively.

$$n = \frac{V^2}{g \cdot \sin\theta} \tag{14}$$

$$n = \frac{g \cdot \sin\theta}{V} \tag{15}$$

All maneuver parameters were analyzed as a function of speed. The stall and maximum velocity of the aircraft was determined, and only between those velocities were the maneuver parameters analyzed.

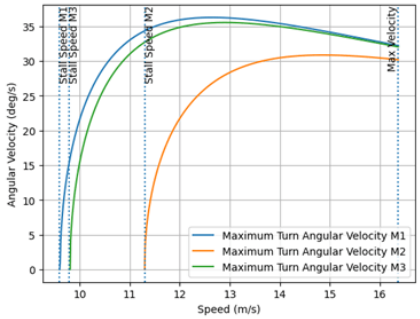

Figure 13: Maximum turning rate for a given air speed.

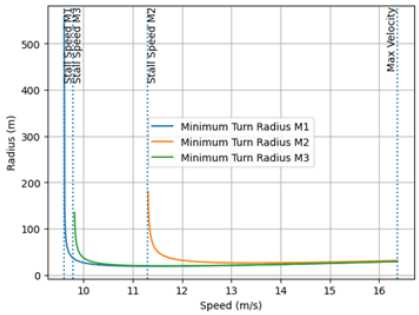

Figure 14: Minimum turning radius for a given air speed.

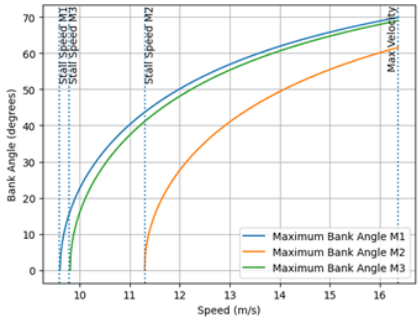

Figure 15: Maximum bank angle for a given air speed.

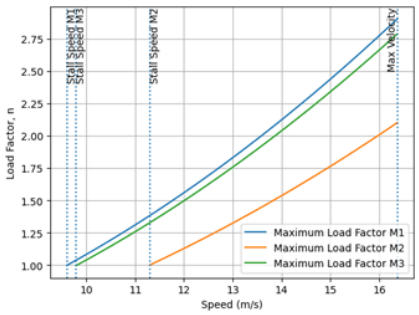

Figure 16: Maximum load factor for a given air-speed.

The team's structural maximum load factor of n = 3, was sustained in all missions. Based on mission goals, maximizing angular velocity yielded the shortest time to complete the turns. However, during turns under load, the effective stall speed changes and the minimum speed to sustain lift, V_corner in Equation (16), was determined as a limitation.

$$V_{corner} = V_{stall} \cdot \sqrt{n} \tag{16}$$

In all cases, the corner velocity was greater than the greatest angular velocity, and therefore the cornering velocity determined the desired bank angle for all missions. Table 18 details desired parameters to complete the turns in the least possible time at corner conditions (left) as well as other mission specific limitations (right).

Mission	Cornering Velocity (m/s)	Cornering Angular Velocity (rad/s)	Corner Bank Angle (°)	Load Factor Limit	Minimum Turning Radius (m)	Maximum Bank Angle (°)
M1	12.70	36.25	54.76	2.90	18.84	69.84
M2	14.95	30.84		2.10	26.04	61.57
M3	12.95	35.52		2.79	19.63	68.97

Table 18: Cornering performance summary.

4.2.3 Velocities and Cruise Feasibility

The optimal glide angle was defined as the pitch angle with the best lift to drag ratio. This was calculated as a mitigation strategy in case the propulsion system failed. Using lift and drag data from flow5, the resulting glide speed is 17.44m/s.

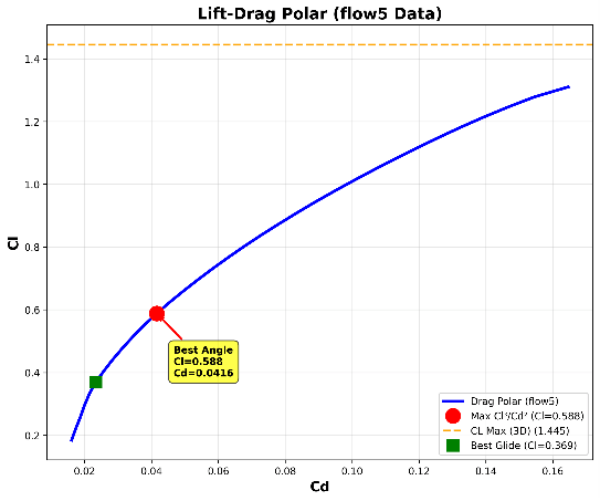

Figure 17: Lift Vs. Drag for Turbo.

The best rate of climb is defined as the velocity with the maximum $\frac{C_L^3}{C_D^2}$ value. This is important as it will allow the aircraft to climb to circuit altitude in the shortest amount of time. This was determined to be 13.81 m/s at a rate of climb of 12.78 m/s, and 4° AOA. Once airborne, to reach a circuit altitude of 200 ft (61 m) at rate of climb V_y, 4.77 s is needed.

$$V_y = V \text{ of } \max\left(\frac{C_L^3}{C_D^2}\right)$$

The maximum possible speed is defined as the point where thrust equals drag. Notably, it is not necessary for the aircraft to fly at this speed, but it is capable of it. Using QAPOT, a cruise speed of 22.20 m/s would yield the same score as flying at the maximum speed since the extra distance would not be sufficient for another lap. The amount of thrust and power available compared to drag and power required is summarized in Figure 18 and Figure 19 respectively. Key velocities are summarized in Table 19.

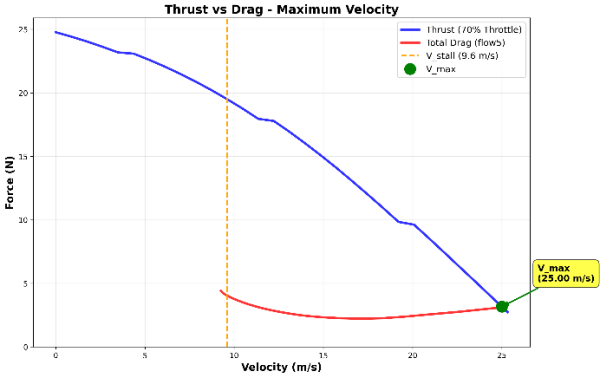

Figure 18: Thrust Available and Drag Vs. Velocity of Envelope of Turbo.

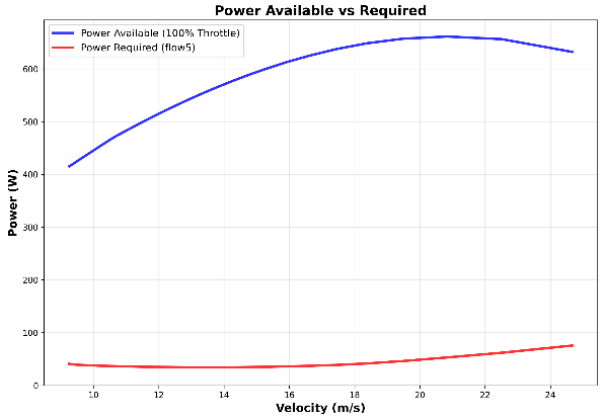

Figure 19: Power Vs. Velocity of Turbo.

Parameter	Velocity [m/s]
V_s, Stall	9.60
V_{glide}, Best glide	17.44
V_y, Best rate	13.81
V_{cruise}, Cruise speed	22.20
V_{max}, Maximum speed	25.00

Table 19: Notable velocities for Turbo.

4.2.4 Takeoff and Landing

Takeoff ground roll was estimated using the same approach as previous DBF reports by approximating the lift-off speed using Equation (17) [5]. Aerodynamic forces during the ground roll were evaluated at the average velocity defined in Equation (18), with drag modeled using Equation (19) and the induced drag factor defined in Equation (20). Rolling resistance was incorporated using the ground friction coefficient defined in Equation (21), applied to the effective normal load $(W - \bar{L})$, where the average lift is given by Equation (22).

$$V_{LO} = 1.2V_{\text{stall}} \tag{17}$$

$$V_{\text{avg}} = 0.7V_{LO} \tag{18}$$

$$C_{D,\text{roll}} = C_{D,0} + kC_{L,\text{max}}^2 \tag{19}$$

$$k = \frac{1}{\pi ARe} \tag{20}$$

$$\mu = 0.040 \tag{21}$$

$$\bar{L} = \frac{1}{2}\rho V_{\text{avg}}^2 S C_{L,\text{max}} \tag{22}$$

$$\bar{D} = \frac{1}{2}\rho V_{\text{avg}}^2 S C_{D,\text{roll}} \tag{23}$$

Using wing area S, the estimated ground roll is $s_{GR} \approx 13.60$ m. This proves that the aircraft can take off safely with the provided runway length. A similar argument can be made about landing.

Parameter	Value
$C_{D,roll}$	0.152
V_{avg}	8.064 m/s
$\bar{L}$	28.75 N
$\bar{D}$	3.088 N

Table 20: Takeoff aerodynamic characteristics of Turbo

$$F_{net} = T - \bar{D} - \mu(W - \bar{L}) \tag{24}$$

$$a = \frac{F_{net}}{m} = \frac{T - \bar{D} - \mu(W - \bar{L})}{m} \tag{25}$$

$$a = 4.88\ m/s^2 \tag{26}$$

Then takeoff distance is

$$s_{GR} = \frac{V_{LO}^2}{2a} = 13.60\ \text{m} \tag{27}$$

4.2.5 Endurance and Predicted Mission Performance

Using QAPOT, a total flight time of 330s is set to account for the 5-minute flight window and an additional 30s for landing. For predicted mission performance, a total time of 280s was allocated by subtracting a 20s roll/climb from the 5-minute time. Effective lap distance as discussed in Section 3.2 was 742 m.

4.2.5.1 M1 & M2

Assuming 100% throttle until cruise conditions at M2 weight, a cruise velocity of 22.2 m/s would yield 8 laps. The battery capacity is capable of an endurance of 11.87 minutes. A full score was predicted for M1, and M2 had a predicted net income of $777.80 with a payload of 21 ducks and 7 pucks.

4.2.5.2 M3 Banner Towing

The banner towing system contributed an additional 174 g to the empty weight detailed in Table 21, for an M3 weight of 4.41 kg.

Part	Mass Per	Quantity
Banner and Rod	61g	1
Servo	10g	2
3D-Printed Mount	60g	1
10” of Rubber Bands	30g	1
Total Banner System Mass	**174g**	

Table 21: Weight of the banner mechanism components.

Disregarding banner drag impact and propulsion limitations at the M3 weight, flying at the maximum possible

cruise speed would not yield an additional lap, therefore the targeted M3 cruise speed was the same as M2. Using Equation (28), the M3 cruise drag coefficient $C_{L,M3\ Cruise}$ was found to be 0.30. Banner drag coefficient using parasitic drag, $C_{D,Banner} = 0.00619$ in Equation (29) determined the overall banner drag coefficient. Equation (30) yielded a total banner drag force of 2.17 N.

$$C_{L,\text{M3 Cruise}} = \frac{2W_{\text{M3}}}{\rho V_{\text{M3,Cruise}}^2 S} \tag{28}$$

$$C_{D,\text{Banner}} = C_{D,0,\text{Banner}} + kC_{L,\text{M3 Cruise}}^2 \tag{29}$$

$$F_{D,\text{Banner}} = \frac{1}{2}\rho V_{\text{M3,Cruise}}^2 S C_{D,\text{Banner}} \tag{30}$$

The overall M3 aircraft drag was 5.41 N. Comparing the new aircraft drag, available thrust and corresponding velocity as discussed in Section 4.2.3, the corresponding cruise velocity under banner drag and M3 weight was determined to be the same as M2 since the drag force remains within the thrust and drag envelope. With a velocity of 22 m/s and the effective lap distance, a total of 8 laps can be completed for M3.

4.2.5.3 Mission Performance Summary

Table 22 summarizes expected mission performance. Since mission scores are dependent on other competitor's performance, which cannot be known, the metric prior to competitor adjustment is shown instead. The ground mission prediction was based off team member feedback.

	M1	M2	M3	GM
Total Mass	4.24 kg	5.85 kg	4.41 kg	4.24 kg
Payload	N/A	21 Ducks, 7 Pucks	55" x 11" Banner	N/A
Laps/Metric	3 Laps	8 Laps	8 Laps	90s Loading Time

Table 22: Expected performance summary.

4.3 Aircraft Stability

4.3.1 Static Stability

After aircraft component sizing, static stability was determined through flow5. The wing and tail section were modeled, and a VLM type analysis was used to determine the neutral point. An initial M1 (no payload) mass estimate was determined by summing the weight of electronics, internal structures, landing gear and carbon fiber skin.

The location of the electronics was not set as the design included a rail system which allowed for the location to be moved if desired. From past team designs, an initial 12% static margin was targeted. Tito had a neutral point of $X_{NP} = 0.169$ m which corresponded to CG of $CG_{desired} = 0.123$ m from the MAC leading edge. Upon construction of Tito, the CG was discovered to be more aft than expected, near the ¾ point of the wing

Component	Weight (kg)
Wing	1.50
Horizontal Stabilizer	0.33
Vertical Stabilizer	0.10
Fuselage	0.53
Landing Gear	0.15
Electronics	1.63
Total Empty Weight	**4.24 kg**

Table 23: Empty weight breakdown.

from the leading edge. For the final design this meant the position of the electronics and M2 payload would have to be farther forward. The aircraft's overall fuselage length was extended and the location of the wing moved aft by approximately 20 cm. The final neutral point is $X_{NP} = 0.21$ m and corresponds to an optimal CG of $CG_{desired} = 0.168$ m for M1. Exact component placement is detailed in Section 5.5.

4.3.2 Trim

Turbo's design is examined in flow5 to determine trim. A sweep of positive and negative angles of incidence for the wing and horizontal stabilizer respectively was conducted using the VLM and type 2 analysis (where weight equals lift). The pitching moment variation with angle of attack and lift coefficient is evaluated. The wing and tail angle of incidence are tuned until the pitching moment is zero at the optimization condition of M1 and M2 cruise averages. This corresponded to an angle of incidence of 1°and -1.75°for the wing and horizontal stabilizer respectively.

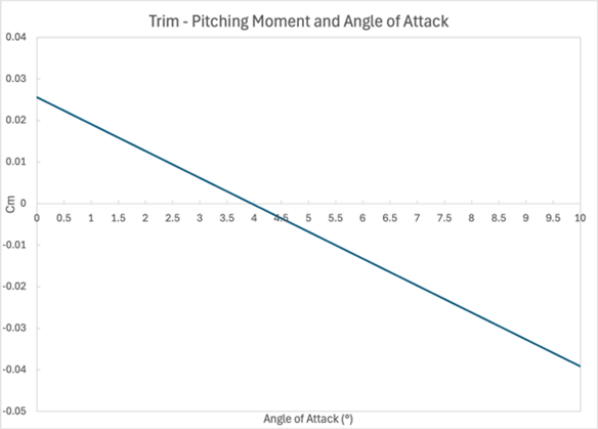

((a)) Lift and Drag Coefficients vs Velocity

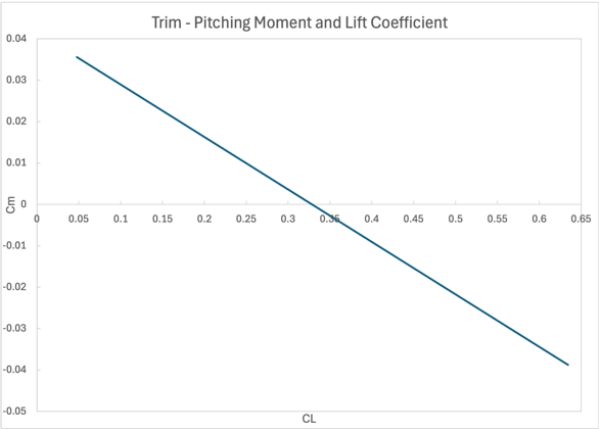

((b)) Drag Components vs Velocity

Figure 20: Trim analysis results.

4.3.3 Dynamic Stability

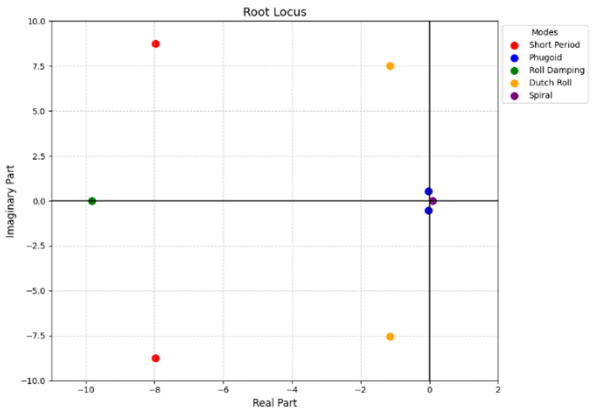

Figure 21: M1 Cruise dynamic stability.

The aircraft's dynamic stability was evaluated in flow5 for the M1 cruise condition under the assumption that other missions would have similar behavior since they share the same targeted static margin. A root-locus plot for the roots of the modes is displayed in Figure 21 where the x axis is stability and y axis is frequency of vibration. For evaluation, stability is marked by a negative real root. Overall, the aircraft is stable in all modes except for the spiral where it is slightly unstable. This can be easily mitigated through pilot correction since the complex roots are very close to zero and the oscillation frequencies are low.

Direction	Mode	ξ [-]	ω [rad/s]	$\lvert\sigma\rvert$ [rad/s]	Time to Half Amplitude [s]
Longitudinal	Short Period	0.674	11.82	7.966	0.087
	Phugoid	0.040	0.521	0.02086	33.23
Lateral	Roll Damping	N/A	N/A	1.829	0.071
	Dutch Roll	0.151	7.61	1.15	0.603
	Spiral	N/A	N/A	0.09453	7.33 *Time to double

Table 24: M1 cruise dynamic stability.

4.3.4 Learnings and Uncertainties

The initial design process was vague to reduce time on computationally heavy methodology and get to manufacturing faster. This was why VLMs were used in place of CFD. While Tito was being manufactured, time was taken for additional research and lessons learned from Tito to inform Turbo. Key lessons included center of gravity, stability and trim. Tito was not trimmed resulting in a non-zero pitching moment across all angles, the CG was not within the predicted range, and stability was not considered. The final aircraft had a different airfoil, was trimmed, had a fuselage length extension, and stability verification.

Two key assumptions were made. Firstly that QAPOT would lead to an optimal starting point and that subsystems were independent of each other. For example, in QAPOT, the team historically determined key parameters such as Oswald's efficiency and taper. Once established, only select aspects were later modified. The second assumption is once the propulsion system was determined to be compatible with the aircraft, it was no longer considered an optimization variable, and its wake was assumed to not impact the rest of the aircraft. Evidently, the wake will impact drag, especially with twin propellors, however, to limit computationally intensive methods, it was neglected. These uncertainties are addressed during flight testing as detailed in Section 7.2.

4.4 Mission Payloads

4.4.1 Passenger and Cargo Restraints

M2 includes several requirements for carrying passengers and cargo as payload. Turbo must be able to carry several passengers, in an upright and level position during flight and they must be fully restrained. To accommodate this, the team came up with several seat designs. The first of the three main designs was inspired by a roller coaster harness where rings will be mounted to the hatch of the passenger compartment. When the compartment is closed, the rings will sit around the passenger necks, restraining them. The second design was inspired by car seatbelts. It consists of mounting outlines of the ducks on the floor of the compartment and placing rubber bands over them to hold them in place. The third design has the ducks sandwiched between the same outlines as before and a compliant material on the roof of the compartment which will conform to the passenger's heads. Since there is far fewer constraints for the cargo, the team plans to 3D-print a minimalistic structure to hold them in place within their compartment. Table 25 shows the weighted evaluation matrix used by the team to choose between the three passenger restraints.

Characteristic	Factor	Roller Coaster Harness	Seat Belt Harness	Sandwich Harness
Weight	0.3	5	4	3
Setup Time	0.3	5	3	5
Restraint Quality	0.4	5	4	5
	1	**5**	**4.1**	**4.4**

Table 25: Weighted evaluation matrix passenger and cargo restraint designs.

The roller coaster inspired design was chosen because unlike the other two proposed designs, it had no obvious flaws in terms of weight, setup time and restraint quality.

4.4.2 Banner Mechanism

In M3 Turbo must be able to takeoff with a banner, deploy it mid-flight and release it before landing. Additionally, the banner must not interfere with flight and not get damaged during the mission. The team considered multiple mechanisms for both the deployment and release phase of the mission. The two main contenders for the deployment phase were a spooling based mechanism and a rubber band release mechanism. The spool mechanism would release the banner by spinning a DC motor, unwinding it like a scroll allowing the wind to pull it to the back of the plane. The rubber band release mechanism involved tensioning rubber bands along the bottom of the fuselage, which holds the banner in place until they are released from one side and are left hanging. There were also two contenders for release mechanisms. The first of which was to hold the string on a disk with an angled hook within the fuselage. The disk would then rotate via servo motor, causing the string to slip off and be released. The second mechanism was similar, except it was a latch which would be actuated by an electromagnet. The latch would consist of a linkage which is mechanically passively locked and would unlock when the magnet was turned on via an over-centering linkage. Table 26 shows the weighted evaluation matrix used by the team to choose between these mechanisms. The team chose to use the rubber band release mechanism and the servo actuated banner release for their simplicity and lower setup time.

Characteristic	Factor	Spool	Rubber Band	Servo Release	Electromagnet Release
Weight	0.3	3	4	4	4
Simplicity	0.2	3	5	5	4
Setup Time	0.2	3	5	5	4
Reliability	0.3	5	4	4	5
	1	**3.6**	**4.4**	**4.4**	**4.3**

Table 26: Weighted evaluation matrix banner mechanism designs.

5 Detail Design

5.1 Dimensional Parameters

The final dimensional parameters are summarized in Table 27.

TURBO					
Wing		**Horizontal Stabilizer**		**Vertical Stabilizer**	
Airfoil	CLARKY	Airfoil	NACA0010	Airfoil	NACA0010
Span	1.5 m	Span	0.672 m	Span	0.180 m
Root Chord	0.425 m	Root Chord	0.210 m	Root Chord	0.210 m
Tip Chord	0.255 m	Tip Chord	0.126 m	Tip Chord	0.126 m
MAC	0.347 m	MAC	0.171 m	MAC	0.171 m
Angle of Twist / Incidence	2° twist w/ +1.00°	Angle of Incidence	-1.75°	Angle of Incidence	N/A
Aspect Ratio	4.40	Aspect Ratio	4.00	Aspect Ratio	1.07
Taper	0.6	Taper	0.6	Taper	0.6
Reference Area (project xy plane area)	0.510 m^2	Reference Area (project xy plane area)	0.113 m^2	Reference Area (project xy plane area)	0.030 m^2
Control Surfaces					
Aileron		**Elevator**		**Rudder**	
Span	0.606 m	Span	0.310 m	Span	0.113 m
LE: x/c %	30	LE: x/c %	40	LE: x/c %	50
Max. Deflection	30°	Max. Deflection	45°	Max. Deflection	45°
Fuselage					
Total Length			1.30 m		
Max. Width			0.150 m		
Max. Height			0.154 m		
Wetted Area			0.410 m^2		
Banner Mechanism					
Banner Width			11”		
Banner Length			55”		

Table 27: Aircraft Geometric Parameters for Turbo

5.2 Structural Characteristics

Turbo's weight and loads were the main consideration in designing and optimizing the structure and subsystems. Although aircraft structure and electronic weight remain constant across all missions, variations in payload weight produce different loading which must be accounted for in structural design. To account for uncertainties in load estimation, manufacturing, and dynamic maneuvers or imperfect landings, a factor of safety of 2 was applied to all critical components. This means that each component is designed to withstand 2 times the expected load. This ensures a durable airframe which is protected against non-ideal landings.

5.2.1 Wing Structure

Figure 22 shows the shear force and bending moment diagrams for one wing, calculated using the M2 aircraft predicted weight and a load factor of 3. The root bending moment represents the critical loading condition. Using the maximum bending moment and Equation (31), a 10 mm diameter carbon fiber spar was initially proposed. However, to increase the factor of safety to 2, the spar diameter was increased to 20 mm.

$$\sigma = \frac{My}{I} \tag{31}$$

Since sourcing a single 1.5 m length of 20 mm carbon rod proved difficult, an alternative solution was implemented. A 1.0 m length of 20 mm rod was extended to the full 1.5 m span by telescoping two 0.40 m lengths of 18 mm carbon rod into each end. This provided the required overall length while maintaining structural continuity and bending strength.

Although the composite skin significantly increases overall wing stiffness and strength, and full wing system analysis indicated a factor of safety greater than 2, the 20 mm spar was retained to ensure a sufficiently stiff structure. Excessive wing deflection could negatively affect the epoxy-bonded joints between the internal structure and the carbon skin, potentially leading to failure and a reduction in structural integrity. Therefore, the larger spar diameter was selected to limit deformation and improve reliability under load.

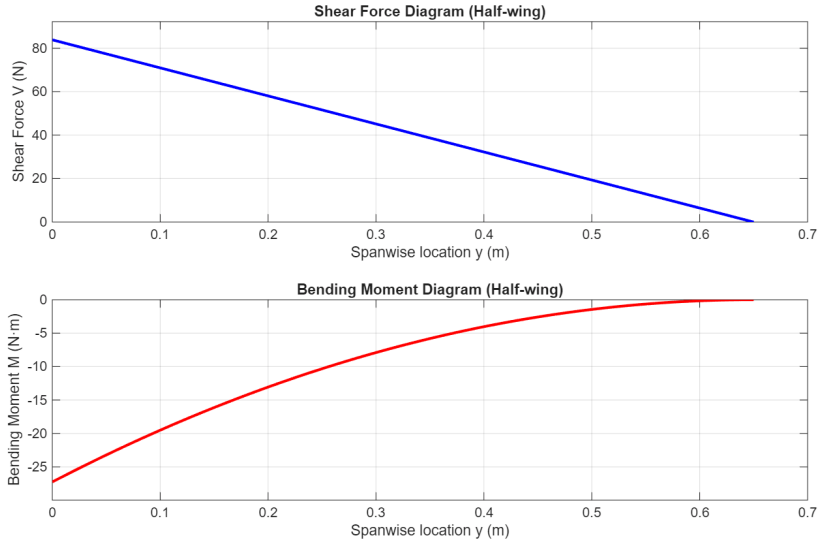

Figure 22: Shear force and bending moment diagrams accross the half-wing span.

For each wing, the carbon rod was placed through 5 ribs, each used to hold the shape of the skin. A plate, with each rib slotted in, runs along the leading edge of the aileron. The plate aligns the ribs and provides a flat plane to glue and bolt the ailerons to the structure.

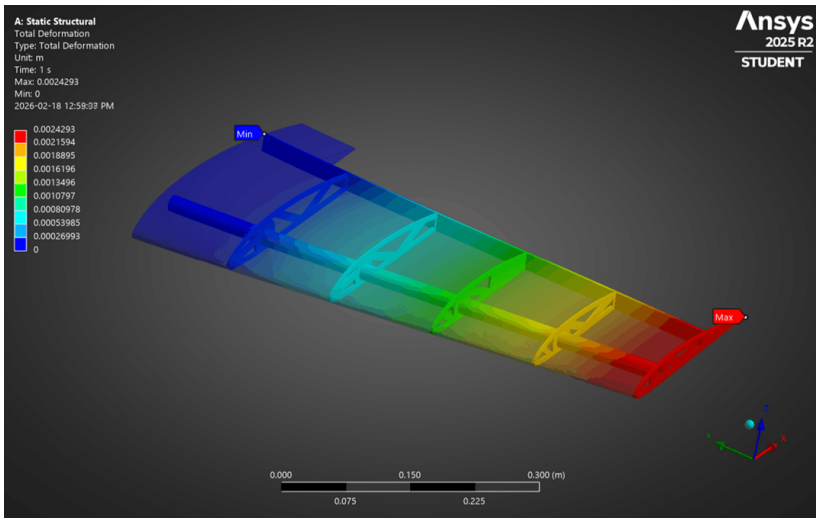

Figure 23: FEA results on the Turbo's wing structure.

Figure 23 shows the applied loading condition: a pressure of 550 Pa at the wing root, decreasing linearly toward the tip. This loading represents the M2 predicted aircraft weight at a load factor of 3, distributed aerodynamically along the span to approximate realistic lift loading. Under this condition, the analysis predicted a maximum deflection of 2.4 mm at the wing tip. This level of deformation is small relative to the 1.5 m span and remains well within the elastic range of the materials.

5.2.2 Tail Structure

The tail structure was designed to minimize weight to shift the CG forward. Figure 24 shows a single 3 mm plywood part connects the horizontal stabilizer and vertical stabilizer. Ribs are epoxied into slots which provide alignment. To further reduce weight, instead of additional ribs at the top of the vertical stabilizer or ends of the elevator, the skin was wrapped and rounded around the edges so that the upper and lower skin halves meet and are bonded together. This creates a closed structure that maintains torsional stiffness and strength.

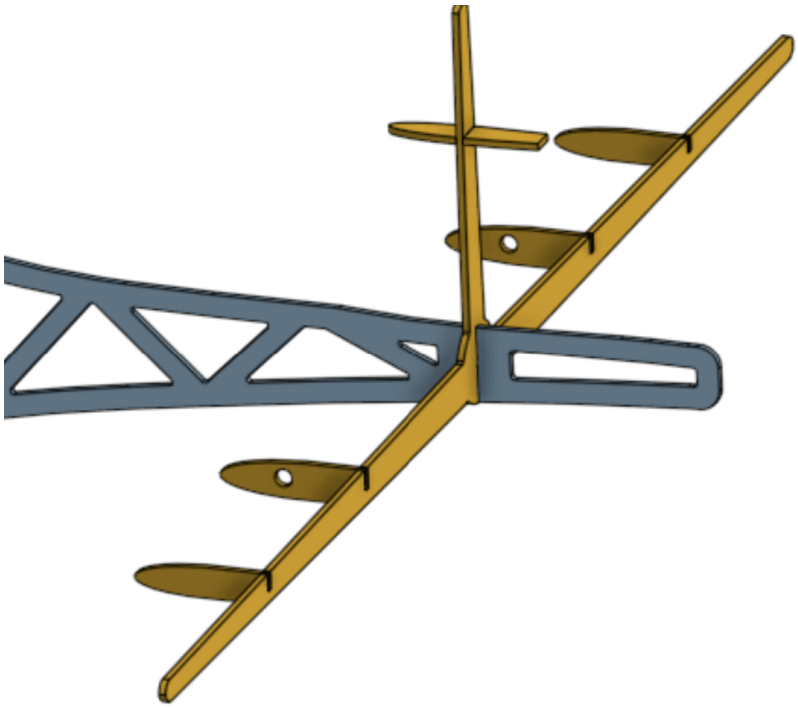

Figure 24: Turbo's tail structure design.

5.2.3 Fuselage Structure

The fuselage structure consists of a flat floor plate and a series of bulkheads that divide the aircraft into functional compartments. These bulkheads also provide mounting locations for components and help maintain overall geometric alignment during assembly.

Due to the tubular cross-sectional shape of the fuselage, the composite skin provides high stiffness and

strength in both bending and torsion. The closed geometry allows the skin to carry shear stresses and resist deformation in all directions. As a result, the internal fuselage structure only serves to separate compartments, support local attachments, and maintain dimensional stability.

5.2.4 Motor Mounts

The two motor mounts were 3D-printed and clamped to the carbon fiber rod between two of the wing's ribs. This allows for the thrust produced loads to be transferred to a primary structural member. Each mount consists of two parts. The bottom half extends the motor out the leading edge while the top half matches the inside shape of the skin. The top half is bonded both to the skin and rod with epoxy reducing the potential for the mount to twist, vectoring the motor in the wrong direction.

Once the top half is glued and a hole is cut in the leading edge, the bottom half can be slid underneath the rod and bolted to the top half and skin using M3 bolts. This two-piece clamping system allows for the motors to be easily removed or exchanged without compromising structural integrity.

To ensure the motor mounts would be capable of withstanding the motor's thrusts, a FEA in Figure 25 was completed on a simplified model. Based on the static thrust test in Section 7.1.2, a maximum force of 11.8N was applied to the mount. Bolts, modeled as rods, showed a maximum stress of 1.76 MPa, well below the allowable stress for the material.

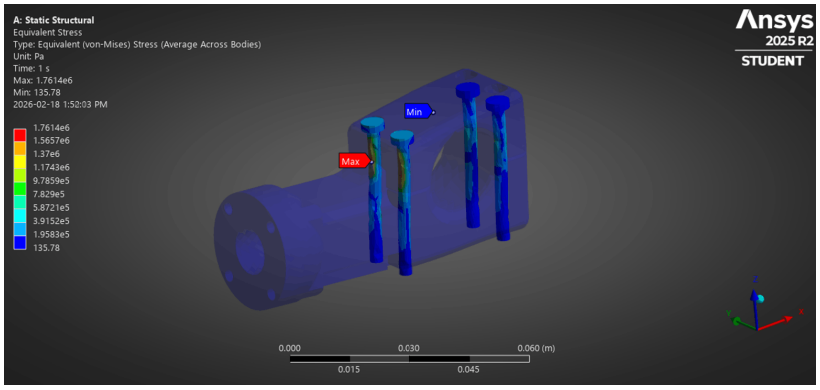

Figure 25: FEA results on the bolts securing Turbo's motor mounts.

To validate the mount itself, bolts and holes were removed and the same 11.8N force was applied. Figure 26 shows the equivalent stress with local maxima between 0.034 and 0.085 MPa. These values are well below the tensile strength of PLA which is often between 40 and 50 MPa [6]. Additionally, the total deformation was simulated to ensure the motor would always be produces thrust in the right direction. Figure 27 shows the bottom mounting plate deforms upward 0.0037mm which is negligible.

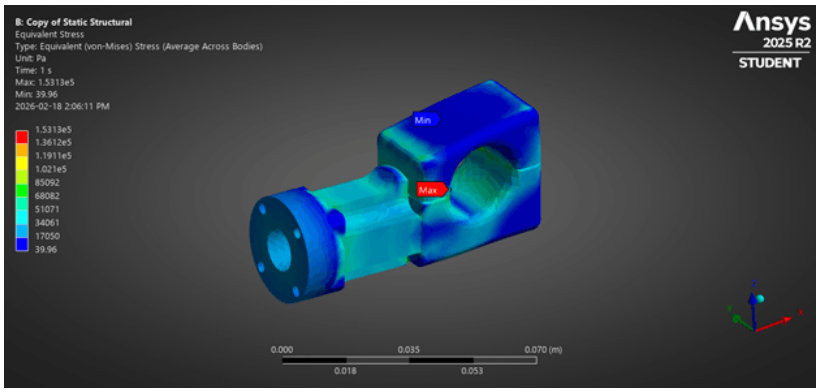

Figure 26: Stress analysis results on Turbo's motor mounts.

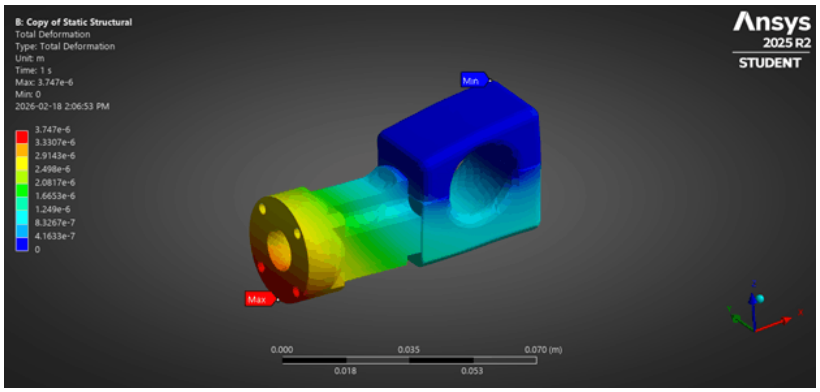

Figure 27: Deformation analysis results on Turbo's motor mounts.

5.2.5 Landing Gear

The landing gear consists of two components. The rear, a 10-layer carbon layup and the front, a 3D-printed. The landing gear must both support the plane on landings and withstand the higher impacts of harder landings. Additionally, if a crash were to occur, the landing gear is designed to fail in a controlled manner as to not disrupt the integrity of the internal structure.

The rear landing gear is arc shaped and was modeled with a wavy pattern to increase bending rigidity. It is composed of two parts, each slotting through a hole in the skin and bolting to the bottom of the fuselage floor plate. If high force were applied vertically to the wheel of the landing gear, a moment will be produced on the bolt and a pull through failure through the floor will occur. This sacrificial failure mode prevents excessive load transfer to the structure, minimizing damage.

Figure 28 shows a FEA stress simulation where a 75 N force is applied vertically to the bottom face with the top face fixed to represent its attachment to the floor. This represents an excessively hard landing. The results show high stress concentration near the interface with the floor. Following hard landings, these locations will be inspected first for damage as they are the most likely locations for fracture.

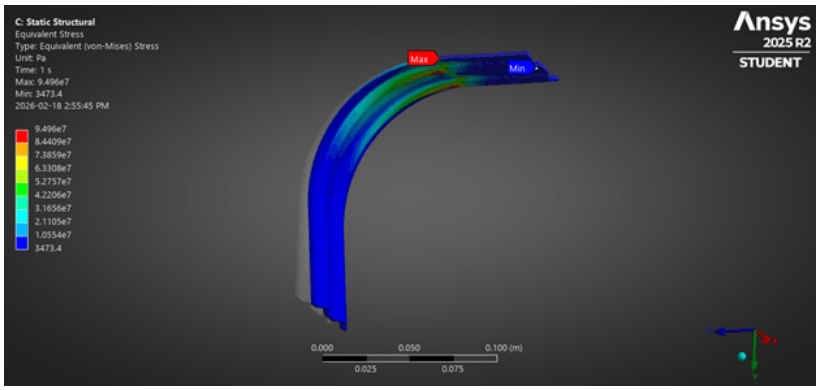

Figure 28: Stress analysis on the landing gear layup.

The front landing gear is 3D-printed and is bolted to the fuselage structure from the top with an M8 bolt and from a bulkhead on its vertical face with two M3 bolts. It extends out of the fuselage through a hole cut in the skin. Like the rear landing gear, the front is also designed to fail before the structure when excessive force is applied. This failure is designed to occur flush with the skin so that if the landing gear were to shear off, the plane would skid on a smooth surface. This is accomplished by reducing the diameter of the landing gear at that location to encourage failure location. If a failure were to occur or different geometry were needed, the landing gear may be removed through the hole after loosening the three accessible bolts.

The front landing gear must withstand all forces associated with landing. These include vertical reaction forces supporting the aircraft weight during touchdown and horizontal forces resulting from runway irregularities, braking, and impact with surface bumps. To ensure structural integrity, a FEA in Figure 29 was completed with a 100 N force acting vertically on the landing gear. Stress concentrations at the gear's two legs are below the UCS of PLA and are located correctly to encourage failure location. The deflection of the two legs outward is mitigated by a solid axle resisting the force.

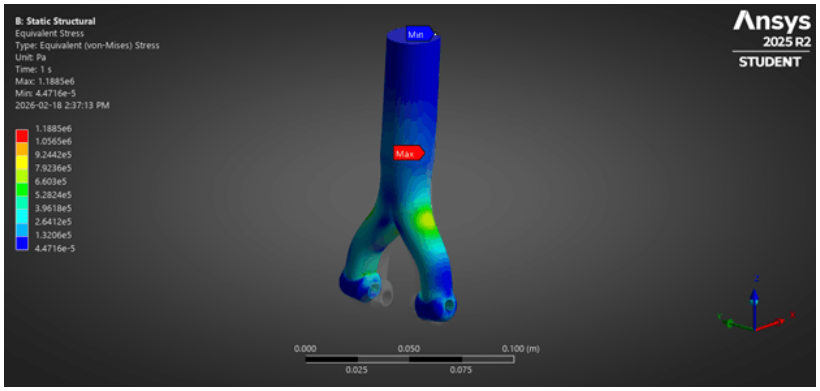

Figure 29: Stress analysis on the landing gear 3D-print.

Next, a 75 N force was applied horizontally to simulate an imperfection in the runway or a nose-first landing. Figure 30 shows the gear deflecting backwards as expected and a stress concentration of 18 MPa close to the skin location. This is also below the expected shear yield strength and in the correct location.

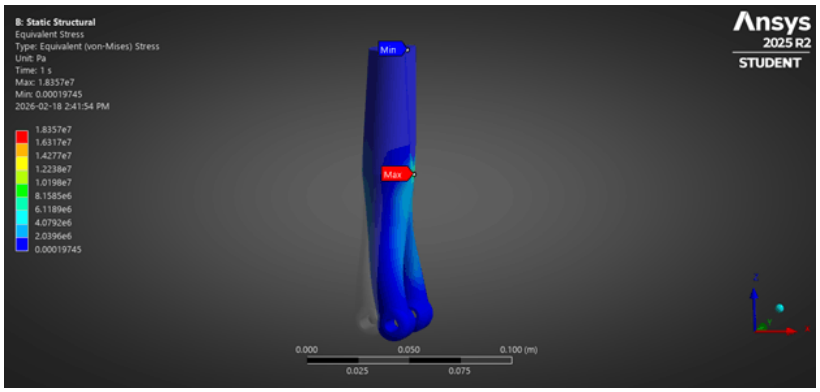

Figure 30: Strain analysis on the landing gear 3D-print.

5.3 Systems Selection and Integration

5.3.1 Avionics

The avionics design can be characterized by three main components the radio receiver, rate gyro and servo motors. To provide communication redundancy the FrSky tandem dual band reciver was chosen for its ability to receive signals on the 2.4 GHz and 900 MHz frequency bands. Historically high winds in Wichita prompted the implementation of the A3 Eagle, a RC flight stabilization solution, which will provide the plane with stabilization on the pitch, yaw, and roll axes. The TGY-813 servos were installed to control all flight control surfaces and banner mechanisms because of its high torque, compact geometry, and reliability. All avionics were powered by a 2S 5300 mAh battery, stepped down to a constant 6V using the FEICHAO 2 – 6S UBEC.

5.3.2 Propulsion

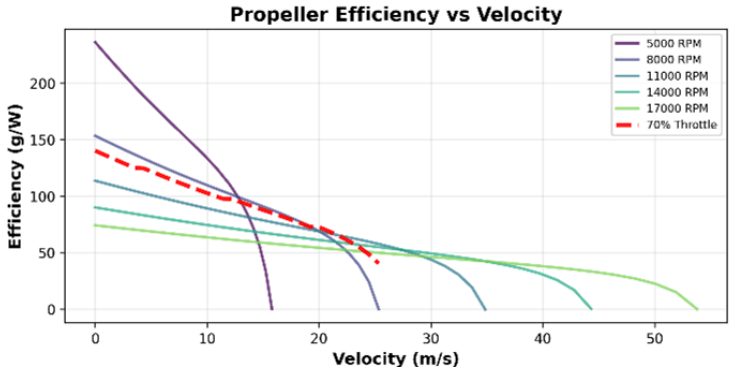

Figure 31: Propeller Efficiency vs Velocity.

The propulsion system consists of two motors, two ESCs and one battery. The propulsion system consists of two motors, two ESCs and one battery. The system is designed around a 3300 mAh 6S lithium polymer battery chosen with reference to the sensitivity analysis. To accommodate thrust requirements at takeoff, two Badass 3515-580 Kv Brushless DC motors were chosen and paired with 10 x 6 wooden propellers from the same manufacturer. Propeller sizing was done by rearranging EQUATION REF for the maximum allowable power draw from each motor over the flight window and the motor specific propeller chart.

$$\frac{1}{2} \cdot E_{available} = \frac{1}{2} \cdot P_{cruise} \cdot 240s + P_{max} * 120s \tag{32}$$

Based on this prop/motor combo and a predicted flight scenario of two minutes at full throttle and four minutes

at cruise throttle, the battery should be able to endure the flight with ~30% of the full capacity remaining. Two Badass 60 A ESCs were used to handle the max current draw from both motors with a FOS of 2.5. Figure 31 shows the propellor efficiency with velocity for the two propellors.

Quantity	Motor	Propeller
2	BadAss BA-3515-580	APC 10x6EW

Table 28: Propulsion components.

5.4 CFD Design Verification

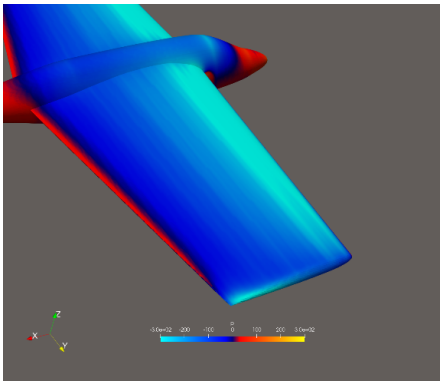

Figure 32: Wing pressure distribution, OpenFOAM CFD simulation for M1.

To verify mission cruise, drag predictions from flow5 were compared with a steady state CFD simulation conducted using OpenFOAM. Due to limited computational resources, only M1 was simulated. The results were a lift and drag coefficient of 0.2956, and 0.0282 respectively. These values were 5.6% and 1.0% off from flow5, and drag force was within the drag/thrust availability envelope, which validated performance expectations prior to physical testing.

Methodology	Lift Coefficient, C_L	Drag Coefficient, C_D
flow5	0.2800	0.0285
CFD	BadAss 0.2956	0.0282
% Difference	5.6%	1%

Table 29: Propulsion components.

5.5 Weight and Balance

Table 30 shows the weight and center of gravity of all of Turbo's components. It also includes mission specific components. The team was able to be very close to the target CG by using the variable battery mount to counter any mission specific weights.

Component	Weight (kg)	CG (m)
Mission 1		
Wings	1.5	0.48
Horizontal Stabilizers	0.33	1.22
Vertical Stabilizer	0.1	1.21
Fuselage	0.45	0.48
Front Landing Gear	0.05	0.64
Rear Landing Gear	0.1	0.93
Avionics Electronics	0.723	0.49
Propulsion Motors	0.382	0.4
Permanent Passenger and Cargo Restraints	0.080	0.23
Propulsion Battery (M1 Placement)	0.525	0.366
Overall Mission 1	**4.24**	**0.543**
Mission 2		
Passengers	0.42	0.5
Cargo	1.19	0.35
Propulsion Battery (M2 Placement)	0.525	0.838
Overall Mission 2	**5.85**	**0.543**
Mission 3		
Banner	0.064	0.83
Banner Mechanism	0.11	0.83
Propulsion Battery (M3 Placement)	0.525	0.271
Overall Mission 3	**4.41**	**0.543**

Table 30: Weight and balance for each mission configuration.

5.6 Aircraft Performance

Turbo's key operating parameters and limitations are shown in Table 31. Although all missions have different weights and therefore slightly different values, the most conservative values across all missions are shown in the table. These parameters guide predicted mission behavior limitations.

Velocities (m/s)	
V_s, Stall	11.30
V_{glide}, Best glide	17.44
V_y, Best rate	13.66
V_{LO}, Lift off	13.76
V_{cruise}, Cruise speed	22.20
V_{max}, Maximum speed	25.00
Angles and Distances	
Stall Angle	13°
Maximum Bank Angle	61.57°
Minimum Turn Radius	26.04 m
Ground Roll	13.60 m
Throttle Settings	
Takeoff (100%)	11209 RPM
Cruise (70%)	8770 RPM
Endurance	
Flight Time at Cruise	11.87 minutes
Weight	
Empty Weight	4.24 kg
Maximum Weight	5.85 kg

Table 31: Conservative operational limits.

5.7 Mission Performance

Table 32 details predicted mission performance and mission specific stall speeds. Notably, all missions have the same target cruise speed since M1 serves to test limitations for future missions while M2 and M3 have the same velocities due to sufficient thrust from the propulsion system. Key score drivers are shown in M2 and M3. QADT predicts a total score of 5.58 for DBF 2026. The largest unknown factor in the total score prediction is the performance metrics of other teams. The team has chosen to predict these metrics based on what is believed to be the maximum achievable performance if a design was solely focused on that aspect of the challenge.

Parameter	M1	M2	M3	GM
Gross Weight (kg)	4.24 kg	5.85 kg	4.41 kg	4.24 kg
Target Cruise Speed (m/s)	22.20 m/s	22.20 m/s	22.20 m/s	N/A
Stall Speed (m/s)	9.60 m/s	11.30 m/s	9.79 m/s	N/A
Time per Lap (s)	35s	35s	35s	N/A
Predicted Performance Metrics	3/3 Laps	21 Ducks, 7 Pucks, 73.26 Wh Total Propulsion Battery Capacity	11” × 55” Banner, RAC = 1	90s Loading Time
Anticipated Laps	3	8	8	N/A
Estimated Max Performance Metrics	N/A	33 Ducks, 11 Pucks, 70 Wh Total, Propulsion Battery Capacity, 10 Laps	15” × 75” Banner, RAC = 0.95, 10 Laps	45s Loading Time
Predicted Mission Specific Score	1.0	Net Income 777.80$	440	90s Loading Time
Predicted Normalized Mission Score	1.0	1.52	2.56	0.5
Total Score	5.58			

Table 32: Predicted Mission Performance

5.8 Drawing Package

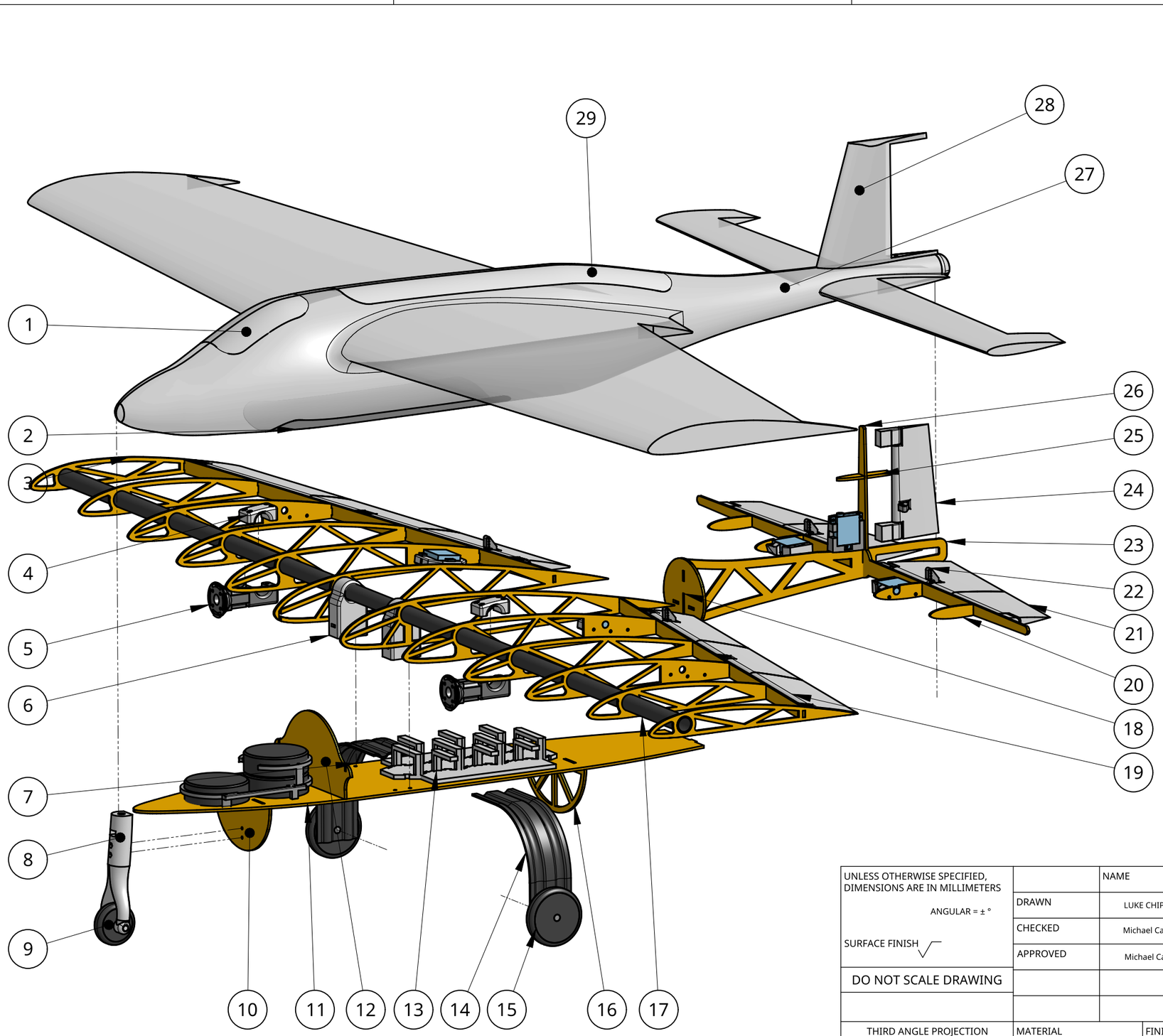

Item	Part	Material	QTY.
1	Puck Hatch	Carbon	1
2	Electronics Hatch	Carbon	1
3	Wing Ribs (Varying Sizes)	3mm Plywood	12
4	Upper Motor Mount	PLA	2
5	Lower Motor Mount	PLA	2
6	Rod Holder	PLA	2
7	Puck Holder	PLA	1
8	Front Landing Gear	PLA	1
9	Front Wheel	TPU	1
10	Front Electronics Bulkhead	3mm Plywood	1
11	Floor Plate	3mm Plywwod	1
12	Cargo Bulhead	PLA	1
13	Duck Holder	PLA	1
14	Rear landing gear	Carbon	2
15	Rear Wheel	TPU	2
16	Back Fuselage Stringer	3mm Plywood	1
17	Wing Spar	18-20mm carbon rods	1
18	Empennage Bulkhead	3mm Plywood	1
19	Aileron	PLA/3mm carbon rod	2
20	Horizontal Stabilizer Spar	3mm Plywood	4
21	Elivator	PLA/3mm carbon rod	2
22	Servo control Horn	PLA	5
23	Empennage Structure	3mm Plywood	1
24	Rudder	PLA/3mm carbon rod	1
25	Rudder Spar	3mm Plywwod	1
26	Tail Structure	3mm Plywood	1
27	Aircraft Skin	Carbon	1

UNLESS OTHERWISE SPECIFIED, DIMENSIONS ARE IN MILLIMETERS

ANGULAR = ± °

SURFACE FINISH

DO NOT SCALE DRAWING

THIRD ANGLE PROJECTION

	NAME	DATE
DRAWN	LUKE CHIPMAN	02/20/2026
CHECKED	Michael Cassidy	02/20/2026
APPROVED	Michael Cassidy	02/20/2026

MATERIAL

FINISH

TITLE

Tito
Exploded View / BOM
Queen's University

SIZE	DWG NO.	REV.
B	2	1

SCALE		SHEET
1:5		1 of 1

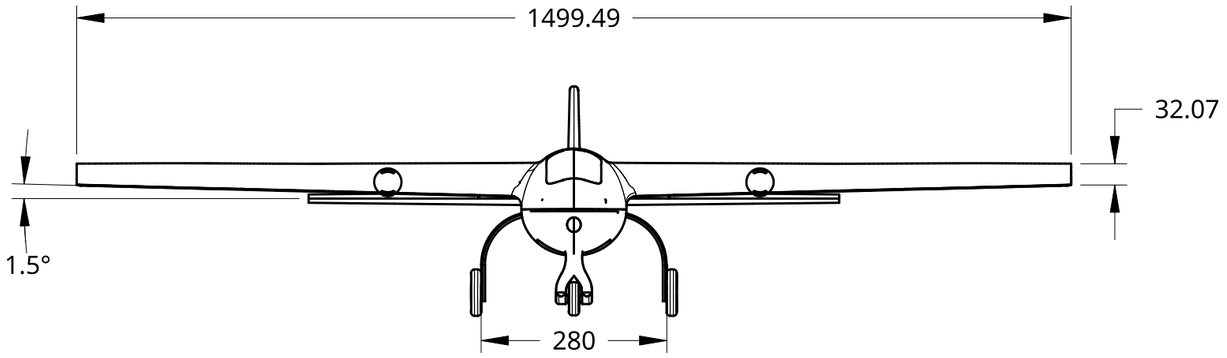

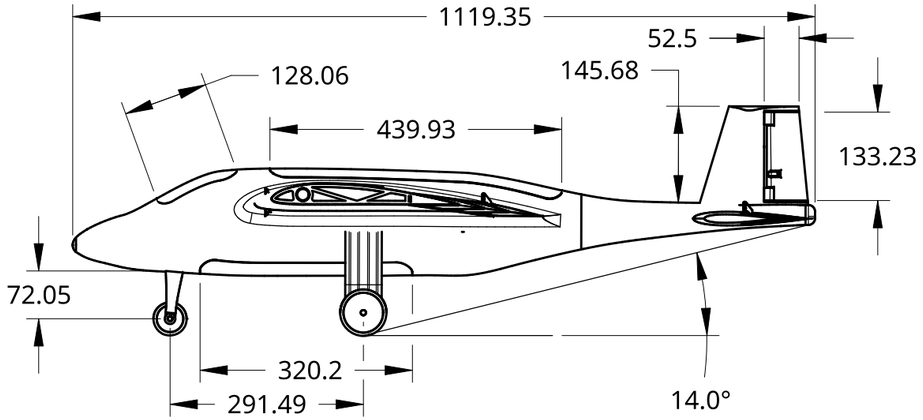

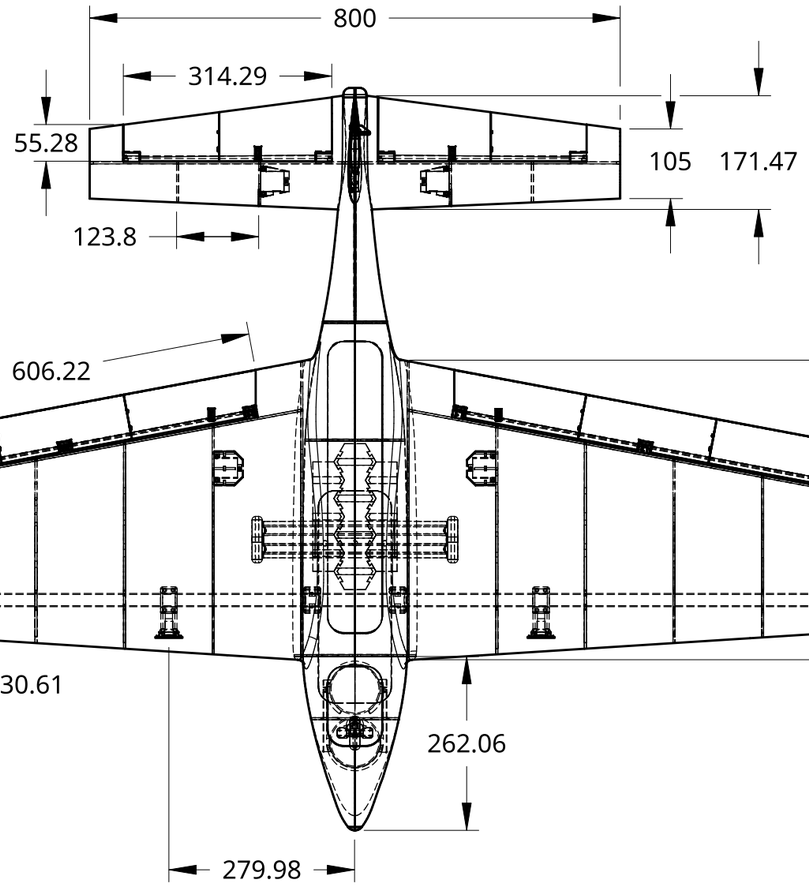

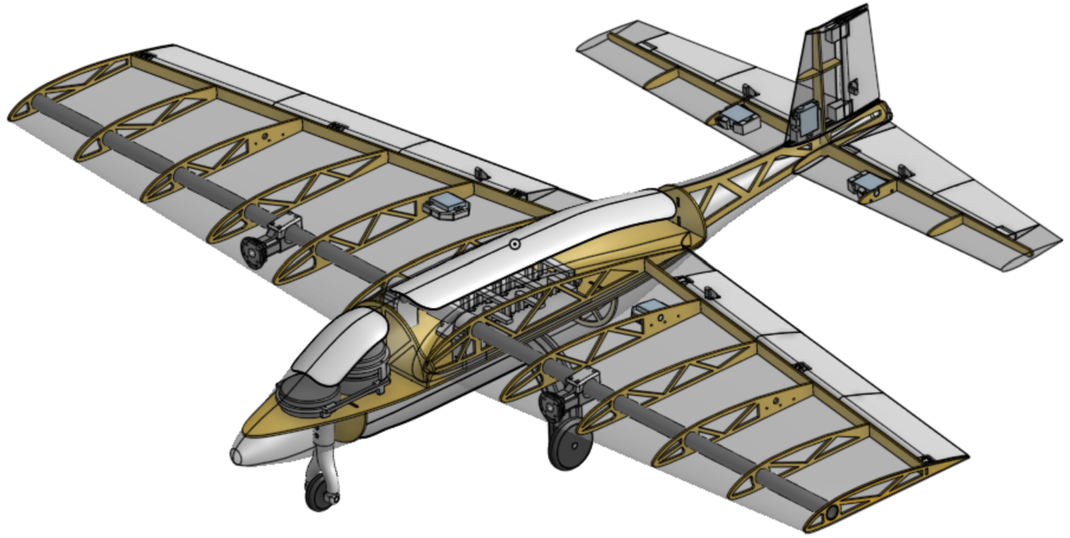

UNLESS OTHERWISE SPECIFIED, DIMENSIONS ARE IN MILLIMETERS		NAME	DATE
ANGULAR = ± °	DRAWN	LUKE CHIPMAN	02/20/2026
SURFACE FINISH	CHECKED	Michael Cassidy	02/20/2026
	APPROVED	Michael Cassidy	02/20/2026
DO NOT SCALE DRAWING			
THIRD ANGLE PROJECTION			

TITLE
Tito
Three View Drawing
Queen's University

SIZE	DWG NO.	REV.
B	1	1

SCALE		SHEET
1:9		1 of 1

6 Manufacturing Plan

6.1 Manufacturing Methods

The team identified available manufacturing processes and potential materials. Each process/material was evaluated on their effectiveness for creating structural components and the opportunity it would provide to develop member skill sets.

6.1.1 Composite Manufacturing

Composites are extensively used in aerospace applications due to their high strength to weight ratio. It is exactly this property which prompted the team to create a composite structure for the planes. Composite parts can either be purchased or manufactured in house. Mass produced parts like carbon rods are cheaper to purchase, but one-offs of any custom shape must be manufactured by the team to reduce cost. The team's manufacturing process for composite parts is a wet carbon layup in 3D-printed molds. Molds are vacuum bagged in order to degas the binding epoxy and to minimize defects like bridging. Composite parts require an investment from the team and are time consuming to make due to mold production and post processing of the parts. While the process limits possible iterations, it gives team members experience in developing composite structures.

For the project, composite parts are highly versatile. Custom parts with simple a design can provide stiffness and toughness with minimal weight. Purchased parts, like carbon rods or plates can create strong, light structural members or internal structure.

6.1.2 CNC Milling

CNC milling is a subtractive manufacturing process capable of cutting a wide range of parts quickly. The team has access to a three axis CNC mill, which is capable of creating vertical cuts in sheet materials. Due to the diameter of the tool head, constraints are placed on possible cuts i.e. no sharp corners. Parts made on the mill are only at the expense of the material. For this application, CNC Milling is best suited for creating wooden parts. Wood's high strength to weight ratio and low cost make it ideal for the internal structure of the plane.

6.1.3 Laser Cutting

Laser cutting is another subtractive manufacturing process often used on thinner sheet materials. Laser cutting is a relatively quick process but is limited by material thickness. Like CNC milling, parts generally need to be two dimensional, limiting design options. The main benefits are all corners are highly dimensionally accurate due to the laser beams small cut width.

Like CNC Milling, Laser cutting may be used to manufacture a wood internal structure. However, its increased accuracy would provide more consistent precise parts.

6.1.4 Water Jet Cutting

Water jet cutting is a cold cutting process which uses a thin stream of water, often mixed with an abrasive, to cut parts. There is a wide range of materials which can be cut with a water jet including carbon fiber plates, another option for a high strength internal structure. Additionally, the mechanism of cut minimizes

mechanical stress which produces a highly dimensionally accurate part. This cutting process does have some drawbacks. Compared to CNC milling and laser cutting, water jet has a higher associated cost and limited availability. This method may be favorable in the case the team uses carbon fiber plates for the internal structure.

6.1.5 Fusion Deposition Manufacturing

Additive manufacturing is a rapid prototyping technology that is very cost effective for one-off parts. Fusion deposition manufacturing (FDM) is a type of additive manufacturing (commonly known as 3D-printing) where molten plastic is extruded in layers in a desired shape and is quickly cooled. Using this method, high strength parts can be achieved by strategically aligning print layers with predicted loading directions. The team has two Bambu Lab X1 Carbon printers which can print a range of polymers. The most cost effective and available is PLA, which although brittle, has high strength at room temperature. TPU is another commonly used polymer, typically used to create flexible structures e.g. landing wheels. Although, FDM has certain drawbacks including size and time constraints with each print taking longer the larger it is and must fit in the build volume of the printer.

3D-printing can create a range of aircraft components. With low density printing or a lightweight plastic, the skin or entire airframe may be printed. It can also be useful create molds if the team chooses to produce a carbon fiber skin. PLA is very effective at making strong mounts for components and structure. And TPU may be used for landing gear or other flexible components.

6.2 Material and Manufacturing Method Selection

Material selection and manufacturing method are closely linked, as certain processes are better suited to specific materials, and certain materials are better suited to particular aircraft components. For this analysis, the aircraft is divided into three primary categories: skin, internal structure, and mounts. Each category has multiple viable material/process combinations.

As discussed previously, some methods are inherently limited in application. FDM printing is the only feasible method for producing complex mounts and will therefore not be directly compared with other processes. Similarly, while water jet cutting is particularly well suited for composite plate, its higher operating cost makes it less competitive for wood or sheet materials; therefore, it will not be directly compared with CNC milling or laser cutting. However, the increased cutting cost associated with composites will be considered when evaluating structural material choices.

Table 33 evaluates manufacturing methods against weight, durability, manufacturing time and member experience criterion. The weight of each figure of merit was determined by considering its alignment with competition goals. Ultimately for the skin, composites were chosen for its weight, durability, and potential experience for members of the team. While the CNC milled and laser cut wood structure tied, CNC milling was chosen for its greater availability to the team. Additionally, since the composite layup process inherently has internal skin inaccuracies, the higher precision of laser cutting was deemed to be unnecessary.

Figures of Merit	Factor	FDM (Skin)	Composites (Skin)	CNC Milling (Wood Structure)	Laser Cutting (Wood Structure)	Water Jet Cutting (Carbon Structure)
Weight	0.4	0.6	0.8	0.7	0.7	0.9
Durability	0.2	0.2	0.9	0.5	0.5	0.9
Manufacturing Time	0.2	0.5	0.2	0.9	0.9	0.1
Experience	0.3	0.5	0.8	0.8	0.8	0.2
	1	**0.53**	**0.78**	**0.8**	**0.8**	**0.62**

Table 33: Weighted evaluation matrix of the available manufacturing methods.

6.3 Manufacturing Execution

6.3.1 Skin

The skin was composed of a two-layer carbon fiber layup forming the outer surface of the wings, fuselage, and tail. The aircraft was split into a top and bottom half to simplify manufacturing and assembly. Using two large continuous layups increased overall rigidity and structural strength while minimizing joints and stress concentrations.

First, 3D-printed negative molds were printed out of PLA, then the carbon was layered into the mold in a wet layup process. Alternating layers of resin and carbon were layed before being placed in a vacuum bag to cure. Typically, the team would sand down the molds to a smooth finish before performing the layups, however, as both an experiment and a time saving measure, the molds were not sanded. Since 3D-printed parts have layer lines, a textured exterior to the skin was expected, which would likely induce extra parasitic drag. However, this was not the case, and the only difference was a more matte surface finish. Four layups were completed for the outer skin; the top and bottom half, hatches, and vertical stabilizer which was glued on in assembly.

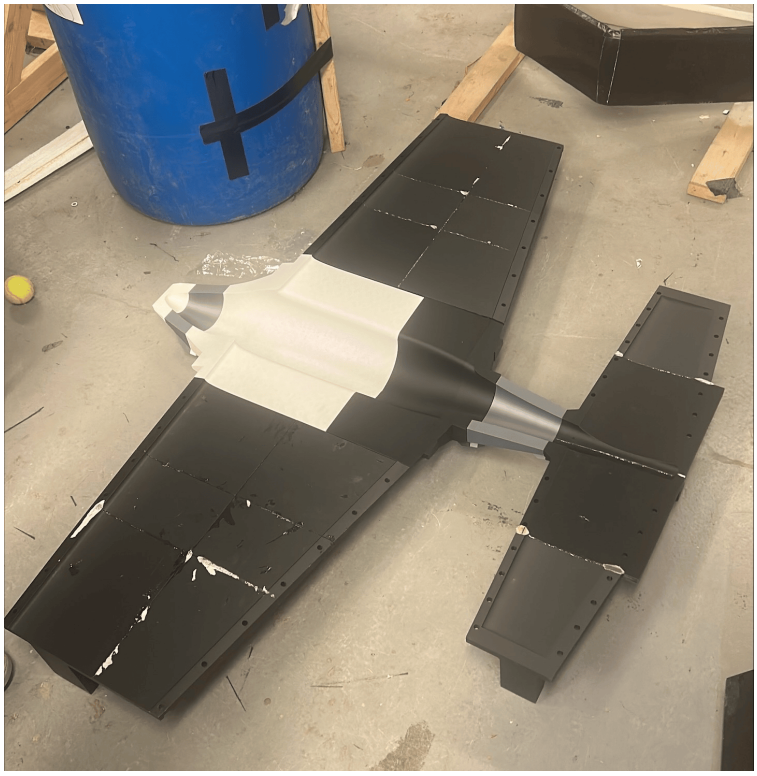

Figure 33: 3D-printed molds to perform the layup.

Figure 34: Laying epoxy on the carbon fiber during the layup process.

Figure 35: Vacuum seal to allow the degas the epoxy.

6.3.2 Structure

Since the skin has high strength and can carry significant loads, the aircraft was designed as a semi-monocoque structure, where both the skin and the underlying framework share the structural load. This approach allows the internal structure to be minimized, serving primarily to maintain the shape of the skin rather than bearing the majority of the stresses. However, this means that the structure cannot support itself. So, with the bottom half of the skin still in the mold, the structure was epoxied together and to the bottom half of the skin before the entire top half was epoxied and placed on top, sealing the plane.

Figure 36: Assembly of the aircraft structure.

The internal structure was CNC milled from 3 mm plywood, which was chosen for its higher strength to weight ratio compared to other options e.g. medium density fiberboard. A 20 mm carbon rod serves as a structural member across the wing and helps align the wing's ribs and the elevation of the floor plate in the fuselage.

6.3.3 Control Surfaces

The control surfaces were 3D-printed using PLA and assembled with a 3 mm carbon rod as the pivot. After the plane was sealed with the structure, locations for the control surfaces on the wings, and tail were cut. The control surfaces were then CA glued to check alignment before being epoxied to the structure and skin.

Figure 37: Control surfaces on Tito.

6.3.4 Landing Gear

The landing gear was manufactured with two materials. 3D-printed TPU was used for the wheels and a carbon layup was used for the structural component. The wheels were printed with exposed infill, providing a mesh-like structure capable of compressing when loaded. The layup for the structural component of the landing gear consisted of ten layers. This layup was an experiment for the team, and the primary goal was to make a part that can withstand high loads of a rough landing. Since epoxy cures with heat and also exothermically reacts after mixing, the part was set and cured very quickly. Due to the large layer count, the structural component has many voids since trapped air could not be properly suctioned out through the additional layers. Initial testing has shown the landing gear can sustain loads ten times greater than the max predicted load.

6.3.5 Component Mounts, Passenger Restraints, Cargo Restraints and Banner Mechanism

The mounts, passenger restraints, cargo restraints and banner mechanism were 3D-printed from PLA. Components were installed using M3 hardware and in some cases with epoxied joints for stronger connections. 3D-printing allowed for rapid prototyping and easy replacement, as the internal layout is adjusted for integration between subsystems.

7 Testing Plan

Subsystem and full flight performance tests were conducted to determine the validity of the design and collect data for iteration/improvement. The tests were subdivided into ground and flight tests which were further subdivided into specific system/characteristics tests. The objective of each test is summarized in Table 34 below.

Test Category	Test	Objectives
Ground Tests	Wing Tip Loading	Observe wing deflection under different load conditions, find maximum structural load conditions
	Static Thrust	Verify manufacturer motor/propeller specifications, find thrust produced at cruise throttle setting (70%)
	Communication Subsystem	Find max operating range of receiver, find optimal receiver placement for constant communication link
	Stabilization Subsystem	Verify stabilization system works as intended, verify configured fail-safe setting works as intended
	Power Subsystem	Verify power system can handle competition load scenarios
	Banner Mechanism	Verify banner mechanism functions as intended
	Speed Loading	Minimize the time required to load passengers and cargo, test different seats/cargo restraints
Flight Tests	Plane Configuration	Verify results from XFLR5 and ANSYS Fluent, verify sizing results found using optimization code
	Take Off Distance	Determine distance required to takeoff with different payload configurations
	Banner Flight	Determine aerodynamic effects of released banner on flight
	Turning Test	Determine turning radius and time
	Banner Release	Verify banner mechanism functions as intended during flight
	Mission Compliance	Simulate competition missions and determine score predictions

Table 34: Ground and flight test plan.

7.1 Ground Testing

Ground testing was completed to benchmark subsystem performance and verify theoretical results. Data collected from ground tests were used to inform subsystem improvements.

Test	Date
Wing Tip Loading	01/12/2026
Static Thrust	01/14/2026
Communication Subsystem	01/15/2026
Stabilization Subsystem	01/17/2026
Power Subsystem	01/19/2026
Banner Mechanism	01/20/2026
Speed Loading	01/20/2026

Table 35: Ground test schedule.

7.1.1 Wing Tip Loading Test

To test the structural strength of the aircraft, a wing tip loading test was done. To conduct the test, the plane was setup between chairs as seen in Figure 38. The air frame was suspended above the ground with the wingtips as the only points of contact to the chairs. Weight was placed on the frame and the structures response was observed. The frame was first tested with the max takeoff weight and then with gradually more weight until noticeable deflection was observed. Wing tip loading tests conducted on Tito were used to inform iterations on Turbo's manufacturing processes.

Figure 38: Apparatus to perform the wing tip loading test.

7.1.2 Static Thrust Test

Static thrust tests were performed to verify the manufacturer's propeller specifications and thrust at 70% throttle (value used in conceptual design). A custom thrust stand was developed using a 3D-printed PLA mount, commercially available load cell, and a microcontroller for data processing/storage. The apparatus was set up as shown in Figure 39. The 10x6 wooden propeller was tested with the Badass 580 Kv DC motor over the entire throttle range. Data collected was compiled into a thrust vs throttle graph and compared with interpolated data used in conceptual design.

Figure 39: Test apparatus for static thrust test.

7.1.3 Avionic Subsystems Tests

Avionics subsystem tests were conducted to verify the proper function of each component/system.

7.1.3.1 Communication Subsystem

Two communication systems tests were conducted to verify the placement of the receiver module and range of operation.

The carbon structure of the plane provides a good medium to block certain radio frequencies including the allowed competition frequencies of 2.4 Ghz and 900 Mhz. The first test was done to verify the placement of the radio receiver. The test was conducted by rotating the plane along all axes to simulate all possible orientations in flight while the transmitter and receiver were connected. If at any point the connection was lost, the antennae/receiver position was adjusted, and the test was repeated.

The second test was done to verify the operational range of the receiver. This test was conducted by placing the plane slightly above the ground. The range test feature mode built into the transmitter was activated and while connected to the receiver, the two were separated. The range test mode changes the power of the output signals, reducing the effective range to 1/30th of the actual. The test was conducted in an open field to avoid signal reflections or blocking.

7.1.3.2 Stabilization Subsystem

The stabilization system was tested to verify the correct direction of stabilization for each control surface, and the preset fail-safe configuration works as intended. To conduct this test, the servos for each control surface were placed roughly corresponding to the correct location in the plane. The rate gyro, receiver, power system, and all servos were connected. The gyro was attached to a separate platform and rotated

exclusively along the pitch, yaw and roll axis and the corresponding deflection of the elevator; rudder and ailerons were observed. At the end of the test the radio connection was terminated, and the gyro fail safe configuration was observed.

7.1.3.3 Power Subsystem

As indicated by the sensitivity analysis, a 3300 mAh battery was chosen, then a propeller and motor combination that was suitable aerodynamically was derived by hand calculation. To justify this sizing approach, a load test was done on the power system to verify that the battery has the capacity to endure the load applied by the motor/propeller throughout flight missions. A custom stand was developed using scrap wood to restrain the motors during the load test, seen in Figure 40. A Pixhawk and its corresponding power module were used to measure and log the electrical characteristics of the battery. Voltage, current, and throttle input data were correlated and analyzed using matplotlib.

Figure 40: Test apparatus created using scrap wood and clamps. Wires taped to the table to avoid them being caught in the blades.

7.1.4 Banner Mechanism Test

Tests were conducted to ensure the reliability of the banner deployment and detachment mechanism to meet M3 and GM requirements. A COTS aircraft owned by the team was used to test the mechanism in flight. A version of the banner mechanism adapted for the COTS plane was 3D-printed for the purpose of the test. Before flight, the mechanism was tested several times on the ground, using a dedicated switch on the transmitter. A flight test is planned to be executed during Tito Flight Day 2 as seen in Table 36. An image of the banner mechanism set up on the test plane can be seen in Figure 41.

7.1.5 Speed Loading Test

The ground mission requires the team to load all passengers and cargo in the plane; points are awarded on the basis of loading speed. To minimize the ground mission time, different passenger seat and cargo hold configurations were tested. The test also informed iterations on the designs that can further minimize the loading time.

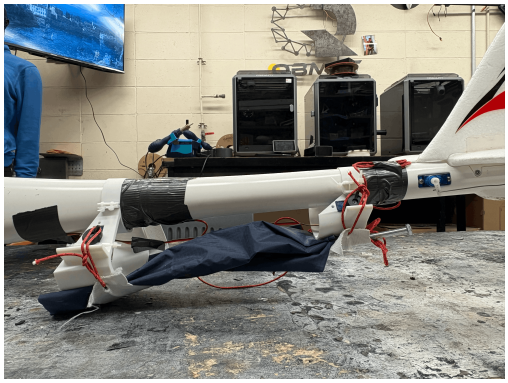

Figure 41: Test apparatus for the banner mechanism created on a test plane.

7.2 Flight Testing

Flight tests were planned to evaluate full system performance and gather data that can be used to inform Turbo's design. Tests were planned to be conducted in two sets, the first done to evaluate Tito's design and the second to verify design improvements based on the results of the first set. The second test set places greater emphasis on mission compliance and pilot training in preparation for the fly-off. A

modular data collection hatch for testing was created which embedded a Pixhawk flight controller, airspeed sensor, power module and angle of attack sensor. Flight logs compiled by the PX4 firmware uploaded to Pixhawk will be used to analyze flight and subsystem performance. The testing methodology follows an increasing risk approach. Tests with a low associated risk to the plane have been planned to be conducted first, and higher risk tasks last. Due to weather conditions in Kingston, Ontario, testing sessions are sparse but densely packed (i.e. multiple test objectives in one session) and will follow the schedule outlined in Table 36. The weather in the team's local area also prompted the creation of 3D-printed skis in place of landing wheels for use in the snow-covered testing field.

Flight		Date	Objective
Tito	Flight Day 1	02/12/2026	Pilot Test
			Trim Tuning
			Stabilization Gain
			Plane Configuration
	Flight Day 2	02/26/2026	Take off Distance
			Turning Test
			Banner Flight
			Banner Release
Turbo	Flight Day 1	03/12/2026	Pilot Test
			Trim Tuning
			Stabilization Gain
			Plane Configuration
			Turning Test
			Banner Flight
	Flight Day 3	03/19/2026	M1 Time Trial
			M2 Time Trial
			M3 Time Trial
	Flight Day 4	04/02/2026	M1 Time Trial
			M2 Time Trial
			M3 Time Trial

Table 36: Flight test schedule.

7.2.1 Flight Checklist

Ground, pre and post flight checks were conducted following the checklist below.

Flight Checklist			
Date			
Flight Crew			
Location			
Weather Observations			
Flight Objectives			
Electrical Inspection		**Post Flight**	
Battery Voltage		Radio Responsive	Y / N
Connections Secure	Y / N	Propellers Intact	Y / N
Battery Secure	Y / N	Skin Intact	Y / N
Mechanical Inspection		Payload Intact	Y / N
Payload Secure	Y / N	Control Surfaces Intact	Y / N
Motors Secure	Y / N	Landing Gear Intact	Y / N
Control Surfaces Secure	Y / N	Motors Intact	Y / N
Landing Gear Secure	Y / N	Battery Intact	Y / N
Skin Intact	Y / N	Battery Voltage	
Pre Flight		**Notes**	
Correct Surface Deflection	Y / N		
Correct Gyro Deflection	Y / N		
Correct Motor Spin	Y / N		
Correct Fail Safe Config	Y / N		
Strong Radio Connection	Y / N		

Table 37: Preflight testing checklist

8 Performance Results

8.1 Subsystem Performance

8.1.1 Static Thrust Test Results

The results from the static thrust test are shown in Figure 42. The data shows a linear correlation, as expected. Although, the magnitude of the thrust produced is much lower than the manufacturer specification and simulated values. At a 70% throttle setting, 1263 grams of thrust were expected from the motor/prop combination. The test indicated that thrust produced at 70% is actually 773.94 grams, resulting in 61.3 % discrepancy between actual and predicted values. Although not expected, the thrust produced at the 70% throttle setting is still sufficient to keep the plane at cruise speed. Some error in the results can also be attributed to the testing methodology. Two-point calibration was used to calibrate the loadcell, but calibrated weights were not available at the time of the test, instead mass of nontraditional weights were approximated and used.

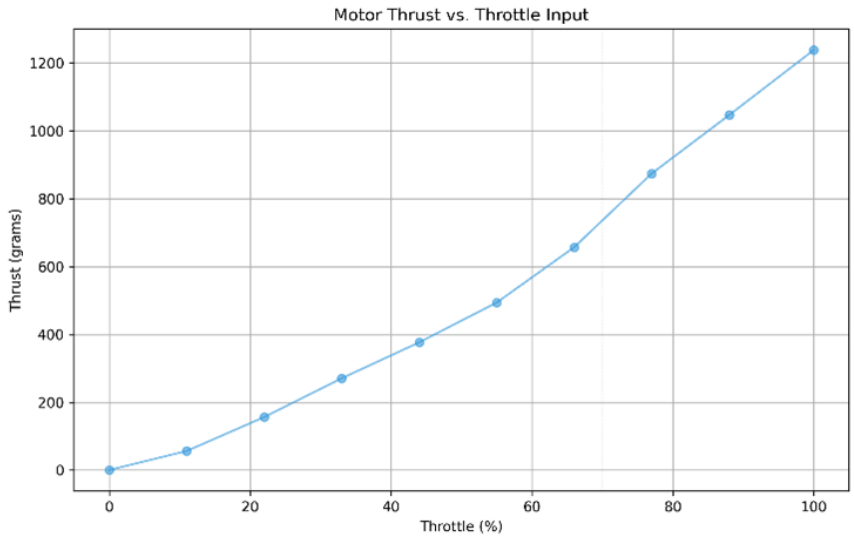

Figure 42: Thrust output in grams vs. throttle input graph created following the procedure outlined in 7.1.2.

8.1.2 Power Subsystem Test Results

The results from the load test can be seen in Figure 43. The graph indicates that the power drawn from the twin motors is 432 W at 70% throttle (cruise throttle setting), 57% above the forecasted value from QAPOT. After re-evaluation it was found that this value, although higher than predicted, does not require the team to buy a new battery for the competition since initial power system evaluation revealed that only 70% of the batteries full capacity will be used over a predicted flight scenario. Based on experimental values the new predicted battery usage is 88%. The now greater battery usage means that there will be a lower FOS in terms of energy requirements during flight and further flight testing should be done to better understand system limits. Note that experimental power data was found in a static scenario, in-flight this value is expected to lower because of the phenomenon known as “propeller unloading” where propeller load is decreased because air is pushed into the propeller.

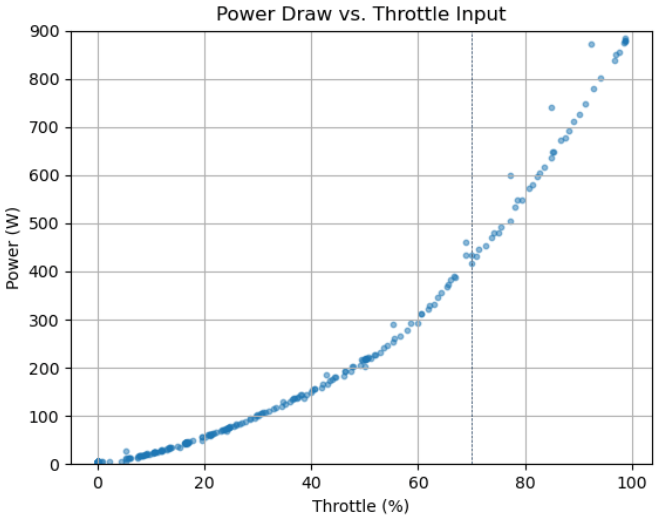

Figure 43: Power draw vs throttle input graph created using experimental data collected following procedure outlined in Section 7.1.3.3.

8.1.3 Communication Subsystem Test Results

Following the procedure outlined in Section 7.1.3.1, tests were conducted to evaluate the radio system. The results of the range test indicated that the receiver has an average operational range of 953 m. This range provides the team with a comfortable area of operation since the competitive flight path only requires that the plane travels a maximum of 152 m (500 ft) away from the start line. A final mounting location under the nose was chosen with antennas pointing outward from the plane at 120-degree increments. Testing showed that this position-maintained connectivity in all realistic air frame orientations.

8.1.4 Wing Tip Loading Test Results

Results of the wingtip loading test showed that the plane structure was able to withstand more than the maximum predicted load of 123 N which was found in Section 4.2.2 with no visible bowing. The max tested load was 20 kg which is significantly higher than the predicted max load. Similar manufacturing processes will be followed for iteration two of the plane so that similar high factor of safety can be achieved.

8.1.5 Speed Loading Test Results

Several time trials were done to determine the best passenger and cargo configuration to minimize loading time and maximize the ground mission score. It was found that the best configuration was to load all cargo in the nose of the plane and place all passengers in the middle. The best passenger hold was determined to be neck constraints, and for the pucks a simple friction constraint. This configuration provided the team with the minimum loading time of 57 seconds.

8.1.6 Banner Mechanism Testing Results

The banner mechanism was extensively tested to ensure that the release mechanism is reliable because it is critical for the M3 score. A banner drop success rate of 95% was achieved over 30 trials with the first iteration of the design. This success rate was satisfactory and no further design changes were made. Instead, consistent loading was practiced so that initial conditions for a successful banner drop are replicated for future trials.

8.1.7 Flight Testing Results

Due to manufacturing delays and local weather conditions only one test session was conducted before the submission of the report. Typically flight tests are conducted at a private field near Kingston, Ontario. At the time of the test, heavy snowfall covered the test field with snow which did not provide a good medium for the plane to take off, even with the addition of the skis. So, reliable flight was not achieved with Tito. An image of the flight-testing grounds and Tito using the skis can be seen in Figure 44. Although no useful quantitative data was obtained from the flight test via the Pixhawk/sensors, the multiple takeoff attempts provided the team with qualitative information that was sufficient for the team to gain confidence in the structural, electrical and aerodynamic characteristics of the plane. Following the flight test plan in Section 7.2, further analysis of the design will be done and used to inform changes for Turbo's design. Qualitative observations gained from the flight test are summarized in Table 38.

Subsystem	Observation	Takeaway
Structure	No visible structural damage after tests	Sufficient structural strength
	Servo horn on control surface detached	Stronger servo horn attachment required
	Entire plane sinking into snow	Larger ski surface area required
Electronics	Sufficient take off speed	Motor/propeller sizing correct
	Insufficient right aileron deflection	Aileron output signal adjustment required
	Right motor disconnected after crash	Stronger/more reliable wire connection required
	Throttle cut switch not stopping both motors	Switch mapping must be confirmed/edited
Aerodynamics	Right rudder input to maintain desired heading	Rudder sizing confirmed
	Nose up attitude during roll / elevator input	Elevator sizing confirmed

Table 38: Flight testing observations and takeaways.

Figure 44: Flight testing setup.

9 Bibliography

[1] Andersen, D., “Understanding Washout,” Model Aviation, March 2012. https://www.modelaviation.com/article/understanding-washout (accessed Jan. 2026)

[2] Joyner, L., “Dihedral Options,” Model Aviation, February 2024. https://www.modelaviation.com/Dihedral-Options (accessed Jan. 2026).

[3] Güzelbey, İ. H., Eraslan, Y., and Doğru, M. H., “Effects of Taper Ratio on Aircraft Wing Aerodynamic Parameters: A Comparative Study,” European Mechanical Science, Vol. 3, No. 1, Mar. 2019. https://doi.org/10.26701/ems.487516

[4] “Introduction to Sweep Angle,” AeroToolbox, https://aerotoolbox.com/intro-sweep-angle/ (accessed Jan. 2026).

[5] University of California, Los Angeles, “AIAA Design/Build/Fly 2024–2025 Design Report,” in Top 3 Design Reports, AIAA Design/Build/Fly 2025, American Institute of Aeronautics and Astronautics, 2025, pp. 64–123. https://aiaa.org/wp-content/uploads/2025/05/Top-3-Design-Reports.pdf (accessed Jan. 2026).

[6] Gao, G., Xu, F., Xu, J., and Liu, Z., “Study of Material Color Influences on Mechanical Characteristics of Fused Deposition Modeling Parts,” Materials (Basel), Vol. 15, No. 19, Oct. 2022. https://doi.org/10.3390/ma15197039.